Bollettino della Società Paleontologica Italiana, 61 (2), 2022, 187-206. Modena

A new physeteroid cetacean from the Lower Miocene of southern Italy: CT imaging, retrodeformation, systematics and palaeobiology of a sperm whale from the Pietra leccese

Emanuele Peri*, Alberto Collareta, Giacomo Aringhieri, Davide Caramella, Luca Maria Foresi & Giovanni Bianucci

E. Peri, Dottorato Regionale Pegaso in Scienze della Terra, Università di Pisa, Via S. Maria 53, I-56126 Pisa, Italy; Dipartimento di Scienze della Terra, Università di Pisa, Via S. Maria 53, I-56126 Pisa, Italy; emanuele.peri@phd.unipi.it *corresponding author
A. Collareta, Dipartimento di Scienze della Terra, Università di Pisa, Via S. Maria 53, I-56126 Pisa, Italy; Museo di Storia Naturale, Università di Pisa, Via Roma 79, I-56011 Calci (PI), Italy; alberto.collareta@unipi.it
G. Aringhieri, Radiologia Diagnostica e Interventistica, Dipartimento di Ricerca Traslazionale e delle Nuove Tecnologie in Medicina e Chirurgia, Università di Pisa, Via Savi 10, I-56126 Pisa, Italy; giacomo.aringhieri@unipi.it
D. Caramella, Radiologia Diagnostica e Interventistica, Dipartimento di Ricerca Traslazionale e delle Nuove Tecnologie in Medicina e Chirurgia, Università di Pisa, Via Savi 10, I-56126 Pisa, Italy; davide.caramella@unipi.it
L.M. Foresi, Dipartimento Scienze Fisiche, della Terra e dell'Ambiente, Università di Siena, Strada Laterina 8, I-53100 Siena, Italy; luca.foresi@unisi.it
G. Bianucci, Dipartimento di Scienze della Terra, Università di Pisa, Via S. Maria 53, I-56126 Pisa, Italy; Museo di Storia Naturale, Università di Pisa, Via Roma 79, I-56011 Calci (PI), Italy; giovanni.bianucci@unipi.it

KEY WORDS - Physeteroidea, Angelocetus cursiensis n. gen. n. sp.*, Mediterranean, Burdigalian, CT-scan, virtual palaeontology, palaeoecology.*

ABSTRACT - Herein we describe a new finding of a medium-sized sperm whale from the Burdigalian (Lower Miocene) of the Pietra leccese formation (southern Italy) on the basis of a partly prepared specimen that includes a partial cranium, seven detached teeth, the fragmentary right mandible and two partial vertebral bodies. Because of the overall compression of the specimen, we carried out a retro deformation of a 3D model of the cranium obtained via CT-scanning. The combined analysis of the original specimen and the retrodeformed model has allowed us to recognise that the studied specimen constitutes a new physeteroid taxon: Angelocetus cursiensis *n. gen. n. sp., a longirostrine sperm whale characterised by a sideward projected supracranial basin, as evidenced by the overall displacement of its posteriormost margin. Based on a phylogenetic analysis,* A. cursiensis *n. gen. n. sp. is determined to be a crown physeteroid that does not belong to either the Physeteridae or the Kogiidae. The wide temporal fossa, elongated rostrum and slender teeth, as well as the skull dimensions (estimated bizygomatic width c. 550 mm) suggest a diet based on medium to large-sized bony fish that were likely captured by a raptorial pierce feeding strategy (as for most of the coeval Burdigalian physeteroids). Despite a seemingly low ecomorphological disparity, the high degree of taxonomic diversity of the Burdigalian physeteroids suggests that this time span represents a crucial phase for the evolutionary history of sperm whales.*

INTRODUCTION

The monuments and historical buildings of the "Barocco Leccese" (XVI-XVIII centuries) are mostly comprised of blocks of limestone from the Miocene Pietra leccese formation of southern Italy (Calia et al., 2014; Margiotta, 2015). Such an intensive use as an appreciated construction stone caused the Pietra leccese limestone to be quarried and subsequently cut into slabs and blocks at several localities of the hinterland of Lecce (Apulia Region). Over the centuries, this quarrying activity has led to discovering a rich fossil assemblage of marine vertebrates that have been described and studied by famous naturalists such as Oronzo Gabriele Costa and Giovanni Capellini (Bianucci & Varola, 2014, and references therein). Starting in the 1980s, an intense collaboration activity between the vertebrate palaeontologists of the Università di Pisa and the late palaeontologist Angelo Varola (†2019) of the Università del Salento (Lecce) led to the discovery, collection, and study of a remarkable number of fossil vertebrates from the Pietra leccese, including the fossil that is described herein.

Due to its poor state of preservation (including the loss of most of the cortical bone) and pervasive fragmentation, the vertebrate fossil dealt with in the present paper was only partially prepared, without proceeding to the removal of the embedding sediment. Moreover, this fossil exhibits an evident degree of post-burial compression. Considering this, we combined direct observations of the exposed portions of the specimen with 3D data resulting from the CT-scanning of the entombed regions. Furthermore, the 3D model of the cranium was digitally retrodeformed to account for the observed degree of compression. The analysis of both the original specimen and the retrodeformed model allowed us to recognise the studied specimen as representative of a new genus and species of sperm whale (Physeteroidea).

Nowadays, only three species of physeteroids are found in the global ocean, all of which are known as highly specialised suction feeders: *Physeter macrocephalus* Linnaeus, 1758 (the largest living toothed whale) and two species of *Kogia* Gray, 1846, namely, *K. breviceps* (Blainville, 1938) and *K. sima* (Owen, 1866) (known respectively as the pygmy and dwarf sperm whale; Werth, 2004, 2006a, b; Bloodworth & Marshall, 2005; McAlpine, 2018; Whitehead, 2018). The situation was different during the Miocene, a time span characterized by an impressive taxonomic diversity and ecomorphological disparity of sperm whales. In particular, the Miocene fossil

record of Physeteroidea includes small- to medium-sized forms that likely fed upon relatively small prey items (e.g., *Cozzuoliphyseteter rionegrensis* [Gondar, 1975], *Rhaphicetus valenciae* Lambert et al., 2020, and many kogiids; Collareta et al., 2017; Benites-Palomino et al., 2020, 2022; Lambert et al., 2020; Paolucci et al., 2021; Bianucci & Collareta, 2022) as well as high trophic level predators that could reach giant body sizes (e.g., *Livyatan melvillei* [Lambert et al., 2010]; Lambert et al., 2008, 2010, 2014, 2017; Boersma & Pyenson, 2015; Benites-Palomino et al., 2022; Bianucci & Collareta, 2022; Kimura & Hasegawa, 2022). Spanning most of the Miocene, the Pietra leccese hosts remains of various sperm whales, including the macroraptorial stem physeteroid *Zygophyseter varolai* Bianucci & Landini, 2006 and the more physeterid-like *Orycterocetus* Leidy, 1853 (Bianucci et al., 2004; Bianucci & Landini, 2006; Peri et al., 2020, 2021). The description of a new physeteroid taxon from the Pietra leccese and the discussion of its phylogenetic and palaeoecological affinities are our main aims here.

GEOLOGICAL AND PALAEONTOLOGICAL FRAMEWORK

The Pietra leccese formation is an informal stratigraphic unit that extensively crops out in the Salento Peninsula (Apulia Region, southeastern Italy) (Fig. 1). This sedimentary unit is mainly formed by yellowish, poorly stratified biomicrites and biosparites that are rich in planktonic foraminifera and calcareous nannofossils (Bossio et al., 2005; Margiotta, 2015). The Pietra leccese transgressively overlies the Upper Cretaceous Calcari di Melissano Formation and the Aquitanian Lecce Formation; upwards, it gradually passes into the Messinian Calcareniti di Andrano Formation that closes the Miocene sedimentary cycle of the Salento Peninsula (Bossio et al., 2006; Mazzei et al., 2009). According to micropalaeontological analyses, the Pietra leccese deposited in an outer shelf palaeoenvironment between the late Burdigalian and the early Messinian (Foresi et al., 2002; Bossio et al., 2005; Mazzei et al., 2009). Although its chronostratigraphic range embraces a time span as long as ca. 11 Ma, the Pietra leccese displays a thickness of only a few tens of meters (Margiotta, 2006; Mazzei et al., 2009). This is explained by the occurrence of several sedimentary hiatuses that are marked by the occurrence of glauconite-rich levels (Balenzano et al., 1994, 2002; Bossio et al., 2005; Margiotta, 2006, 2015; Mazzei et al., 2009).

Fig. 1 - Location of the site where the *Angelocetus cursiensis* n. gen. n. sp. holotype (MSNUP I-16954) was found (Cursi village, white star) on a schematic regional geological map of the Salento Peninsula (Apulia, southern Italy). Brownish areas indicate the outcrops of the Pietra leccese, the calcareous formation from which the studied fossil originates. Scale bar equals 20 km. Redrawn and modified after Calia et al. (2014).

The (macro)palaeontological importance of the Pietra leccese mostly relies on its exceptional content of fossil marine vertebrates, including cetaceans, sirenians, turtles, crocodiles, and bony and cartilaginous fishes. Cetaceans are one of the most diverse groups, including both odontocetes (toothed whales) and mysticetes (baleen whales) (Bianucci & Varola, 2014). The toothed whales are represented by *Eurhinodelphis* aff. *bossi* (Kellogg, 1925), "*Eurhinodelphis*" *salentinus* (Moncharmont Zei, 1950), *Schizodelphis* sp. (Eurhinodelphinidae), *Hesperoinia dalpiazi* Moncharmont Zei, 1956 (Inioidea?), *Messapicetus longirostris* Bianucci et al., 1992 (Ziphiidae), *Rudicetus squalodontoides* (Capellini, 1878) (Kentriodontidae), *Squalodon* sp. (Squalodontidae), *Orycterocetus* sp. and *Zygophyseter varolai* (Physeteroidea), as well as by fragmentary remains of Inticetidae, Kentriodontidae and Physeteroidea (Moncharmont Zei, 1950, 1956; Menesini & Tavani, 1968; Bianucci et al., 1992, 1994, 2016; Bianucci & Varola, 1994, 2014; Lambert, 2004; Bianucci & Landini, 2006; Peri et al., 2019, 2020, 2021). Fossil baleen whales from the Pietra leccese include the holotype of *Archaeschrichtius ruggieroi* Bisconti & Varola, 2006 (Eschrichtiidae), fragmentary remains of Balaenidae, and putative members of Cetotheriidae (Bianucci, 1996; Bisconti & Varola, 2006; Bisconti, 2008; pers. obs.). The sirenian record includes remains of *Metaxytherium medium* (Desmarest, 1822) (Dugongidae) (Bianucci et al., 2003). Chelonians are represented by *Psephophorus polygonus* von Meyer, 1847 (Dermochelyidae), *Trachyaspis lardyi* von Meyer, 1843 (Cheloniidae) and indeterminate cheloniids (Chesi et al., 2007). Crocodilians include specimens referred to Tomistominae indet. and Crocodylia indet. (Aldinio, 1896; Capellini, 1897; Kotsakis et al., 2004). The bony fishes include members of Istiophoridae (*Makaira* Lacépède, 1802), Scombridae (*Acanthocybium* Gill, 1862 and *Scomberomorus* Lacépède, 1802), Fistulariidae (*Fistularia* Linnaeus, 1758), Serranidae, Holocentridae and Molidae (Carnevale et al., 2002; Collareta et al., 2021). Cartilaginous fishes are represented by abundant dental remains and much rarer skeletal specimens belonging to several genera of Carchariniformes, Lamniformes, Myliobatiformes and Rhinopristiformes (Vigliarolo, 1890; Menesini, 1969; Sorce, 2009). In addition to these body fossils, the Pietra leccese also hosts marine vertebrate digestichnia such as coprolites and gastroliths (Tavani, 1973; Collareta et al., 2019b; Collareta et al., in press).

MATERIAL AND METHODS

Institutional abbreviations

IRSNB: Institut Royal des Sciences Naturelles de Belgique, Bruxelles, Belgium; MAS: Museo Arqueologico de Salango, Salango, Ecuador; MAUS: Museo dell'Ambiente, Università del Salento, Lecce, Italy; MGPUF: Museo di Storia Naturale, Sezione di Geologia e Paleontologia, Università degli Studi di Firenze, Firenze, Italy; MLP: Museo de La Plata, La Plata, Argentina; MNHN: Muséum National d'Histoire Naturelle, Paris, France; MSNC: Museo Civico di Storia Naturale di Comiso, Comiso, Italy; MSNUP: Museo di Storia Naturale, Università di Pisa, Calci, Italy; MUSM: Museo de Historia Natural de la Universidad Nacional Mayor de San Marcos, Lima, Peru; MUSNAF: Museo di Storia Naturale dell'Accademia dei Fisiocritici, Siena, Italy; USNM: National Museum of Natural History, Smithsonian Institution, Washington DC, USA.

Studied specimen

The partial sperm whale skeleton MSNUP I-16954 (Fig. 2) was recovered by Angelo Varola from a quarry in the outskirts of the village of Cursi (Fig. 1). The bones comprising the specimen were entombed in six contiguous slabs of Pietra leccese limestone: five slabs (measuring 388 mm in length, 371 mm in width and 39 mm in thickness) were superimposed on each other; the sixth slab (measuring 515 mm in length, 371 mm in width and 39 mm in thickness) was placed anteriorly. For the slab positioning, a hiatus of ca. 15 mm between adjacent slabs was assumed during the preparation of the specimen. Such a gap, filled by mastic (grey layers in Fig. 2) represents the amount of rock that was lost during the cut. The mechanical preparation of MSNUP I-16954, made by the late Angelo Varola, resulted in freeing from the limestone matrix most of the dorsal surface of the neurocranium (from the preserved apex of the nuchal crest to the ventral part of the temporal crest). Hence, in dorsal view, parts of the maxillae, premaxillae, presphenoid (nasal septum) and nasal (all of which form the supracranial basin) are visible. Posteriorly, the supraoccipital is also partly exposed, whereas the left temporal fossa is largely visible in lateral view. Five teeth from the same specimen were also extracted from the sediment. The ventral surface of the cranium and part of the left zygomatic process of the squamosal (the right one is missing) are still embedded in the limestone slabs and have been described herein on the basis of the 3D model resulting from the CT-scan. The fragmentary mandible and the few preserved postcrania of MSNUP I-16954 are also known from the CT images only.

Specimens analysed for comparison

In addition to MSNUP I-16954, we have directly examined for comparison the following extinct and extant physeteroids: *Acrophyseter deinodon* Lambert et al., 2008 (MNHN SAS 1626); *Acrophyseter robustus* Lambert et al., 2017 (MNHN PI 239); *Acrophyseter* sp. (MUSM 2182); *Aprixokogia kelloggi* Whitmore & Kaltenbach, 2008 (USNM 187015); *Cozzuoliphyseter rionegrensis* (MLP 62-XII-19-1; MLP 62-XII-18-1); *Diaphorocetus poucheti* (Moreno, 1892) (MLP 5-6); *Eudelphis mortezelensis* (Du Bus, 1872) (IRSNB M.523); *Kogia breviceps* (MAS 4000; MNHN 1976-37; USNM 283625); *Kogia danomurai* Benites-Palomino et al., 2021 (MUSM 3888); *Kogia pusilla* (Pilleri, 1987) (MGPUF 1540V); *Kogia sima* (MSNC 3450; MUSNAF Mam410); *Koristocetus pescei* Collareta et al., 2017 (MUSM 888); *Livyatan melvillei* (MUSM 1676); *Orycterocetus crocodilinus* Cope, 1867 (USNM 22926¸ USNM 14730); *Orycterocetus* sp. (MAUS 29/1); *Placoziphius duboisi* Van Beneden, 1869 (IRSNB M.530); *Physeter macrocephalus* (MNHN 1831; MSNUP 265, 266, 267); Physeteroidea indet. (MSNUP I-17076); *Physeterula dubusi* (Van Beneden, 1877) (IRSNB M.527); *Platyscaphokogia landinii* Collareta et al., 2020 (MUSM 3291; MUSM 3405); *Pliokogia apenninica* Collareta et al., 2019a (MSNUP I-17603); *Rhaphicetus valenciae* (MUSM 2543); *Scaldicetus caretti* Du Bus, 1867 (IRSNB M.512); *Scaphokogia cochlearis* Muizon, 1988 (MNHN PPI 229, MUSM 971, MUSM 1998); *Scaphokogia totajpe* Benites-Palomino et al., 2020 (MUSM 973); *Scaphokogia* sp. (MUSM 972); *Thalassocetus antwerpiensis* Abel, 1905 (IRSNB M.525); *Zygophyseter varolai* (MAUS 229/1).

Imaging and retrodeformation

The CT-scan analysis was performed at the Cisanello University Hospital (Pisa, Italy). The acquisition parameters were the following: space between slices, 0.625 mm; slice thickness, 0.625 mm; tube voltage output, 140 kV; tube current, 525 mA. For CT data visualization and processing, we used the open-source software package 3D Slicer. To improve the contrast at the interface between the rock matrix and the entombed bones, we filtered the CT images through an adaptive histogram equalization. This filter generated a large amount of noise, which was reduced by applying an anisotropic diffusion filter. Such a processing improved the quality of the CT-scan, thus allowing for a better interpretation of the images. Due to the low difference in density between the limestone and the entombed fossil bones, no automatic threshold-based algorithm was able to recognise the bony elements. Consequently, we manually segmented the CT images based on texture differences between the fossil bone and the entombing rock matrix by using the "paint" tool of 3D Slicer to create masks representing the skeletal elements of MSNUP I-16954. Wherever possible, we used differently coloured masks for different bones. Finally, we exported the segmented masks as .stl files, thus obtaining a digital model of MSNUP I-16954.

The compression that affects the skull of MSNUP I-16954 is mainly dorsoventrally directed; consequently, the whole cranium appears as distinctly flattened. To estimate the degree of post depositional compression, we initially assumed that the preserved foramen magnum was originally circular. We verified this hypothesis by calculating the ratio between the height and the maximum transverse width of the foramen magnum in 37 extant odontocete species (two Kogiidae, one Physeteridae, four Ziphiidae, 28 Delphinidae and two Monodontidae) and 11 fossil odontocete species (five Kogiidae, one crown Physeteroidea and five stem Physeteroidea). We plotted the resulting values in a box plot that is provided in the Supplementary Online Material 1 (SOM 1), Fig. S1. The sample mean of these ratios is 0.97 (closely approaching 1, i.e., the ratio displayed by a perfectly circular foramen magnum), and the standard deviation is 0.11. Based on

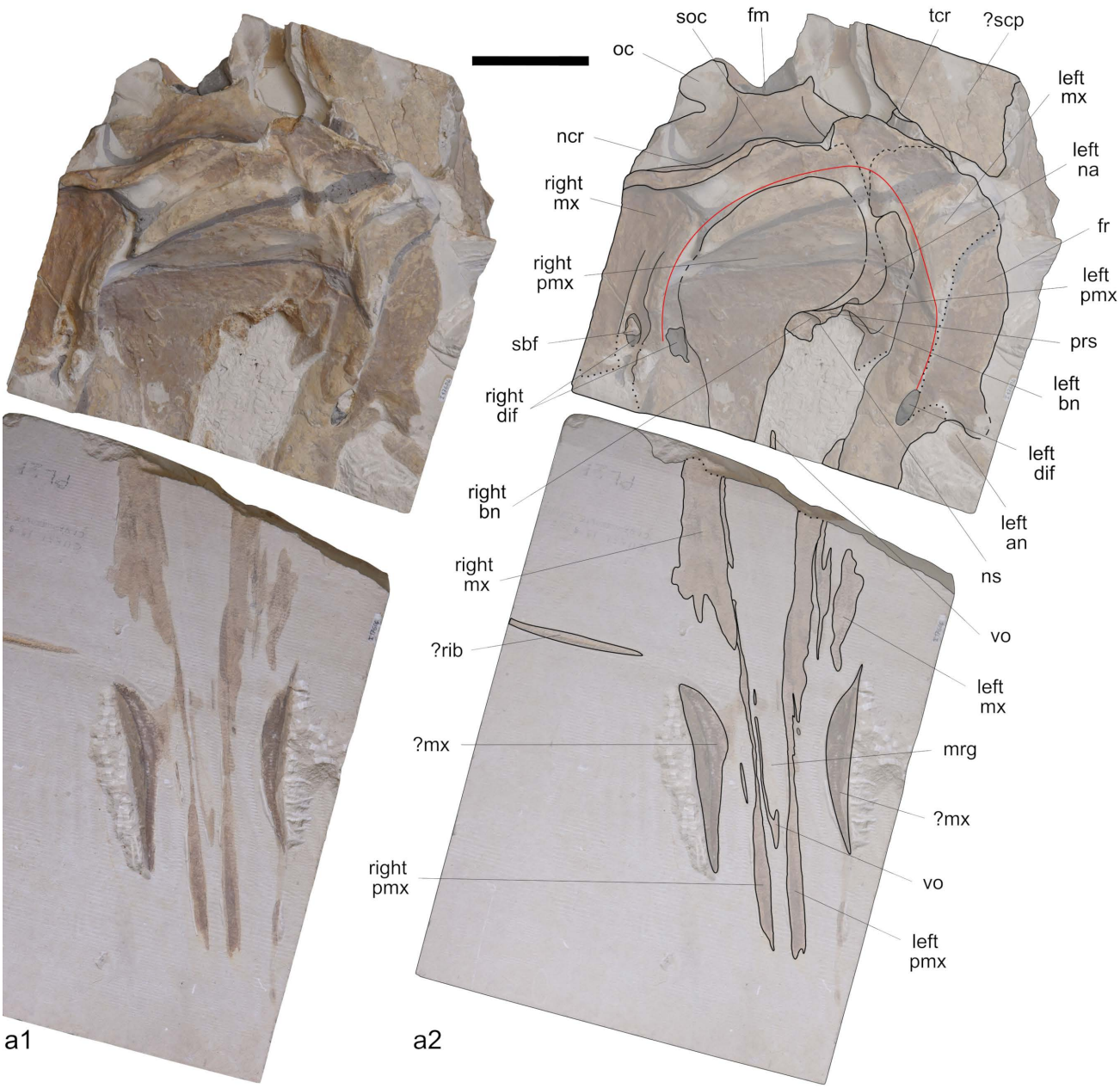

Fig. 2 - Cranium, in dorsal view, of *Angelocetus cursiensis* n. gen. n. sp. (MSNUP I-16954, holotype) from the Burdigalian (Lower Miocene) of the Pietra leccese. Photograph (a1) and explanatory line drawing (a2). The grey-shaded areas indicate the presence of foramina. The stippled lines indicate reconstructed bone margins. The dotted lines indicate broken/eroded margins. The red line indicates the preserved margins of the supracranial basin. Scale bar equals 100 mm. An: antorbital notch; bn: bony naris; dif: dorsal infraorbital foramen; fm: foramen magnum; fr: frontal; mrg: mesorostral groove; mx: maxilla; na: nasal; ncr: nuchal crest; ns: nasal septum; oc: occipital condyle; pmx: premaxilla; prs: presphenoid; sbf: superimposed bony fragment; scp: scapula; soc: supraoccipital; tcr: temporal crest; vo: vomer.

these data, we concluded that the assumption of a circular shape of the foramen magnum is well founded for MSNUP I-16954. To operate the retrodeformation of the cranium, the most diagnostic preserved anatomical district, we imported the 3D models of MSNUP I-16954 obtained from the CT-scan into the open-source software Blender. To reverse the dorsoventral compression, we scaled the digital model of the skull along the dorsoventral axis. We also slightly scaled the skull along the transverse (i.e., mediolateral) axis in order to correct a weak degree of right lateral displacement that is particularly evident on the supraoccipital. Then, in Blender, we joined the retrodeformed meshes to form a unique 3D model of the MSNUP I-16954 skull; and the latter was subsequently exported as a .stl file to facilitate the view of the final product on free and open-source 3D softwares (Fig. 3). Thus, the description provided here for MSNUP I-16954 is based on the prepared portions of the original specimen, on the 3D model extracted from the CT images, and on the retrodeformed 3D model.

Phylogenetic analysis

We coded the osteological features of MSNUP I-16954 into the matrix published by Lambert et al.

(2017) with the additions made by Benites-Palomino et al. (2020, 2021), Collareta et al. (2020), Alfsen et al. (2021), Lambert et al. (2020) and Kimura & Hasegawa (2022). We also added a new character (c. 54) describing the transverse extent of the supracranial basin across Physeteroidea. The final matrix includes 34 taxa, three of which are outgroups (*Cynthiacetus peruvianus* Martinez-Cáceres & Muizon, 2011, *Zygorhiza kochii* [Reichenbach in Carus, 1847] and *Agorophius pygmaeus* [Müller, 1849]), and 54 morphological characters. The list of characters and character-taxon matrix used in our cladistic analysis are provided in the SOM 2. The phylogenetic analysis was undertaken with PAUP* 4.0.a169 (Swofford, 2002). We used the tree-bisection-reconnection algorithm and the heuristic search option. All characters were considered as unordered and unweighted.

SYSTEMATIC PALAEONTOLOGY

Cetacea Brisson, 1762
Odontoceti Flower, 1867
Physeteroidea Gray, 1821

Angelocetus n. gen.

Etymology - The genus-level name honours the late Angelo Varola, prominent Italian palaeontologist who substantially contributed to the current knowledge on the Pietra leccese fossil assemblage by discovering, preparing, and describing many vertebrate specimens.

Type and only known species - *Angelocetus cursiensis* n. sp.

Diagnosis - Same as for the type species until other species are described.

Known range - Lower Miocene (Burdigalian) of southern Italy.

Angelocetus cursiensis n. sp.
(Figs 2-7)

Etymology - The specific name recalls the village of Cursi, the type locality of *A. cursiensis*.

Holotype and only known specimen - MSNUP I-16954, an incomplete skeleton consisting of an almost complete cranium, seven detached teeth, the fragmentary right mandible, and two partial featureless vertebral bodies.

Type locality and age - MSNUP I-16954 was found in 1988 at a limestone quarry in the vicinities of the Cursi graveyard (geographic coordinates: 40° 09'09''N, 18°18'29''E) (Lecce Province) (Fig. 1). The foraminiferal content of the limestone entombing MSNUP I-16954 allows for bracketing the age of this specimen between the FCO (First Common Occurrence) and LCO (Last Common Occurrence) of *Paragloborotalia acrostoma* (Wezel, 1966) (19.52 and 16.74 ± 0.5 Ma, respectively) (Lirer et al., 2019), and consequently to the Burdigalian. Considering that the Pietra leccese spans chronostratigraphically between the upper Burdigalian and the lower Messinian (Foresi et al., 2002; Bossio et al., 2005; Mazzei et al., 2009; Margiotta, 2015), MSNUP I-16954 originates from the lower portion (i.e., Lower Miocene) of the Pietra leccese.

Diagnosis - *Angelocetus cursiensis* n. gen. n. sp. is unambiguously recognized as a member of Physeteroidea due to its broad supracranial basin and strongly asymmetric external bony nares. It differs from members of the family Kogiidae by the absence of a sagittal facial crest. *Angelocetus cursiensis* n. gen. n. sp. differs from all other extinct and extant non-kogiid physeteroids known to date by virtue of its strongly eccentric supracranial basin, which is markedly shifted posterolaterally toward its left side. It is further diagnosed by the following character combination: rostrum elongated (rostral length/condylobasal length 0.62 or higher), supracranial basin extended onto the rostrum, maximum width of the cranium comprised between 400 mm and 600 mm (estimated bizygomatic width about 550 mm), antorbital notches located outside the supracranial basin, two large right dorsal infraorbital foramina occurring close to the corresponding antorbital notch, presence of a single nasal, supracranial basin not extending onto the right orbit, right premaxilla reaching the sagittal plane on the posterior wall of the supracranial basin, frontal/maxilla suture forming an angle between 15° and 35° (25°-32° on the retrodeformed model) in lateral view posterior to the antorbital notch, postglenoid process of the squamosal more ventrally developed than the posttympanic process, absence of a wide notch posterior to the postglenoid process, occipital shield almost flat, maximum tooth diameter smaller than 5% of the maximum cranium width, presence of an unornamented enamelled crown, mandibular condyle placed slightly posterodorsal to the angular process, and dorsal margin of the temporal fossa much lower than the cranial vertex.

Angelocetus cursiensis n. gen. n. sp. differs from the closely related physeteroids *Diaphorocetus poucheti*, *Orycterocetus crocodilinus*, *Placoziphius duboisi* and *Thalassocetus antwerpiensis* by the postglenoid process being more ventrally developed than the posttympanic process. Moreover, *A. cursiensis* n. gen. n. sp. differs from *O. crocodilinus* and *Thalassocetus* spp. by having a right dorsal infraorbital foramen piercing the floor of the supracranial basin and an anteroposteriorly longer temporal fossa (about 60% of the neurocranium length, versus 45%-48% in *O. crocodilinus* and 37% in *Thalassocetus* spp.); from *D. poucheti* and *O. crocodilinus* by the larger teeth (average maximum width 17.1 mm, versus 10.3 mm in *D. poucheti* and 8.9 mm in *O. crocodilinus*); from *O. crocodilinus* by the enamelled dental crown and the absence of a large dorsal infraorbital foramen piercing the right margin of the supracranial basin; from *D. poucheti* by the neurocranium not dorsoventrally flattened, the antorbital notch not reduced to a narrow slit, and the roughly rectangular paroccipital process (triangular in *D. poucheti*); from *P. duboisi* by having a wide right dorsal infraorbital foramen bordering the lateral margin of the supracranial basin; from *Thalassocetus* by the wider skull

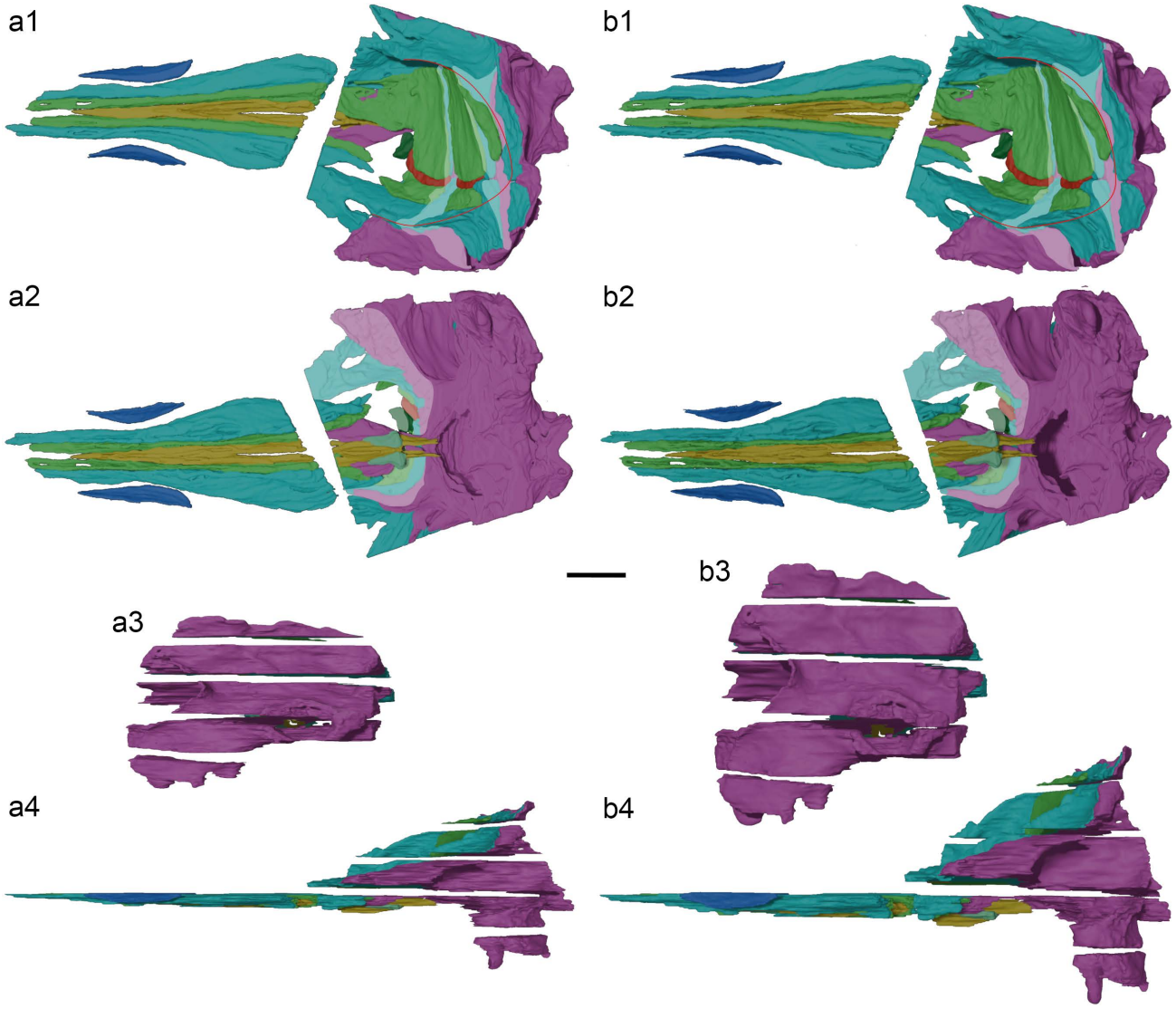

Fig. 3 - Comparison between the cranial 3D models of *Angelocetus cursiensis* n. gen. n. sp. (MSNUP I-16954, holotype) before (a1-4) and after (b1-4) the retrodeformation in dorsal (a1, b1), ventral (a2, b2), posterior (a3, b3) and lateral (a4, b4) views. The white-shaded areas indicate cut surfaces on the neurocranium. The red line indicates the preserved margin of the supracranial basin. Scale bar equals 100 mm. Light blue: maxilla; light green: premaxilla; yellow: vomer; dark green: presphenoid; red: left nasal; aquamarine: pterygoid; pink: neurocranium.

and the convex suture between the right maxilla and nasal (concave in *Thalassocetus*).

DESCRIPTION

Ontogeny

The teeth of *Angelocetus cursiensis* n. gen. n. sp. have open pulp cavities (Fig. 7b1), which coupled with the limited degree of apical wear of the crowns may suggest a young ontogenetic age for this sperm whale individual (Evans et al., 2002). However, it is worth underlining that in the physeteroids the closure of the pulp cavity does not always occur, not even in adult individuals. For example, adults of *Physeter macrocephalus* and *Kogia* spp. retain open pulp cavity, whereas the teeth of the holotype of *Zygophyseter varolai* (possibly an adult individual) exhibit closed pulp cavity (Boschma, 1938; Bianucci & Landini, 2006; Lambert et al., 2017; Lambert & Bianucci, 2019).

Body size estimation

The body length of *Angelocetus cursiensis* n. gen. n. sp. is here estimated at 4.54-4.91 m by applying the two equations proposed by Lambert et al. (2010), which in turn are also based on measurements of *Zygophyseter varolai*. We obtained these values on the basis of the preserved condylobasal length (837.5 mm) and the estimated bizygomatic width (550 mm). Considering that a small part of the rostrum is probably missing, the calculated body size is somewhat underestimated. All things considered, we regard a body length of about 5 m as realistic for *A. cursiensis* n. gen. n. sp. Interestingly, through the same equations, Lambert et al. (2020) obtained similar body length values (4.71-5.05 m) for the roughly coeval Peruvian species *Rhaphicetus valenciae*.

Preservation state

The anterior portion of the rostrum, the dorsalmost portions of both the premaxilla and maxilla along most of

the rostrum, and parts of the right side of the neurocranium and ascending process of the left maxilla were lost due to saw-cutting of the Pietra leccese slabs. The ventral surface of the cranium was eroded before the final burial. The cortical bone is locally preserved but mostly lost due to pre-burial erosion. As reported above, the cranium suffered a strong, dorsoventrally oriented post-burial compression.

Overall cranial morphology

In dorsal view, the outline of the cranium of *Angelocetus cursiensis* n. gen. n. sp. appears as grossly drop-shaped. This is mostly due to the shape of the rostrum, which is broad at its base and distinctly tapers anteriorly. The rostrum appears as distinctly elongated. This is supported by the ratio between the preserved rostral length and condylobasal length (rostral index), which is equal to 0.62, characterising *A. cursiensis* n. gen. n. sp. as a longirostrine form according to the scheme proposed by McCurry & Pyenson (2019). Once again, it should be noted that the rostrum apex is missing; considering the morphology of its preserved portion, the length of the missing part cannot be easily estimated. The rostral morphology of *A. cursiensis* n. gen. n. sp. contrasts with that observed in physeteroids like *Cozzuoliphyseter rionegrensis* and *Diaphorocetus poucheti*, in which the rostrum is short, displaying a bottlenecked appearance in dorsal view.

The supracranial basin of *A. cursiensis* n. gen. n. sp. does not expand transversely, differing from some physeteroids like *Acrophyseter* spp. and *Zygophyseter varolai* in which the supracranial basin also extends onto the right orbit. The preserved lateral margin of the supracranial basin extends about 60 mm anterior to the level of the antorbital notch, thus suggesting that such a concavity was originally not limited to the neurocranium, although its anterior extension cannot be reconstructed in detail due to the poor preservation of the rostrum. Nevertheless, two bone fragments, taking their place respectively on the right and left sides of the rostrum and interpreted herein as dislocated portions of the maxillae, display a dorsal surface that is clearly laterally bent, suggesting a dorsally convex rostrum. Considering the morphology of the preserved supracranial basin and on the bony fragments referred to the maxillae, the supracranial basin of *A. cursiensis* n. gen. n. sp. extends overs the dorsal surface of the rostrum, surpassing the extension observed in more stemward taxa such as *Rhaphicetus valenciae*. Moreover, the supracranial basin of *A. cursiensis* n. gen. n. sp. exhibits an unusual strong displacement towards the left side of the skull that generates a marked skull asymmetry. (Fig. 3a1, b1). On the retrodeformed model, the supraoccipital shield appears as almost vertically oriented, culminating in a high nuchal crest (Fig. 3a4, b4). In this respect, *A. cursiensis* n. gen. n. sp. recalls physeteroids (e.g., *Orycterocetus crocodilinus* and *Physeter macrocephalus*) having a dorsoventrally elevated cranium. At the same time, *A. cursiensis* n. gen. n. sp. differs from several other physeteroids like *Rhaphicetus valenciae* and *Eudelphis mortezelensis*, which display a lower elevation of the nuchal crest, and consequently, a lower cranium.

The preserved left antorbital notch is placed outside the supracranial basin and appears as broadly opened. However, considering the large missing portion of the left maxilla, the precise outline of the left antorbital notch cannot be ascertained. Despite this fracture, the condition observed in *A. cursiensis* n. gen. n. sp. seems to differ from that observed in other physeteroids in which the antorbital notch is reduced to a narrow slit (e.g., *Livyatan melvillei* and the scaphokogiines).

On the retrodeformed model (Fig. 3b4), in lateral view, the temporal fossa of *A. cursiensis* n. gen. n. sp. is wide and slightly longer than high. This cranial feature appears as much more developed than in the extant physeteroids *Kogia* spp. and *P. macrocephalus*, which display a reduced temporal fossa. Moreover, the temporal fossa of *A. cursiensis* n. gen. n. sp. is proportionally longer anteroposteriorly (ratio between the length of the temporal fossa and the length of the neurocranium equal to 0.61) than that of *A. morricei* (0.26) and *O. crocodilinus* (0.45-0.48), but proportionally higher than in *R. valenciae*. Similar to the condition observed in other physeteroids such as *Kogia* spp., *O. crocodilinus*, *P. macrocephalus* and *R. valenciae*, but unlike *Acrophyseter deinodon*, in *A. cursiensis* n. gen. n. sp. the temporal fossa does not reach the top of the skull and the nuchal crest.

Premaxilla

The dorsal surface of the rostral portions of the premaxillae is largely lost due to saw-cutting of the limestone slabs; in turn, within the supracranial basin, the premaxillae appear as deeply abraded due to pre-burial erosional processes. In dorsal view (Figs 2 and 4a1), both the premaxillae are transversely narrow up to about 17 cm from the base of the rostrum; here, the right premaxilla widens transversely to become more than three times wider than the left premaxilla at the base of the rostrum. The widening of the posterior rostral portion of the right premaxilla regards the medial portion of the bone, which forms a medial projection that partly roofs the mesorostral goove. Posterior to this prominence, the medial margin of the right premaxilla displays a wide notch that forms the lateral and posterolateral margins of the right bony naris. Posterior to the latter, the right premaxilla projects posterodorsally to form the ascending process. The latter is greatly expanded toward the left side of the cranium, reaching a maximum transverse width of about 147 mm. Such an expansion of the right premaxilla covers a large part of the posterior wall of the supracranial basin. The right maxilla/premaxilla suture is well discernible, especially considering the CT images. On the posterolateral portion of the supracranial basin, the right premaxilla does not reach the top of the nuchal crest, being separated from the latter by a posteromedial exposure of the right maxilla. This condition resembles that observed in several physeteroids (e.g., *Aprixokogia kelloggi*, *Miophyseter chitaensis* Kimura & Hasegawa, 2022, *Orycterocetus crocodilinus* and *Physeter macrocephalus*) in which the maxilla and/or a small portion of the frontal separate the right premaxilla from the supraoccipital, but differs from *Acrophyseter deinodon*, *Acrophyseter robustus* and several Kogiidae, in which the right premaxilla reaches the top of the nuchal crest. The suture between the right premaxilla and the nasal, although only partly discernible both on the original specimen and in the CT-scan, appears as medially bowed, like in *A. robustus*, *Idiophyseter merriami*

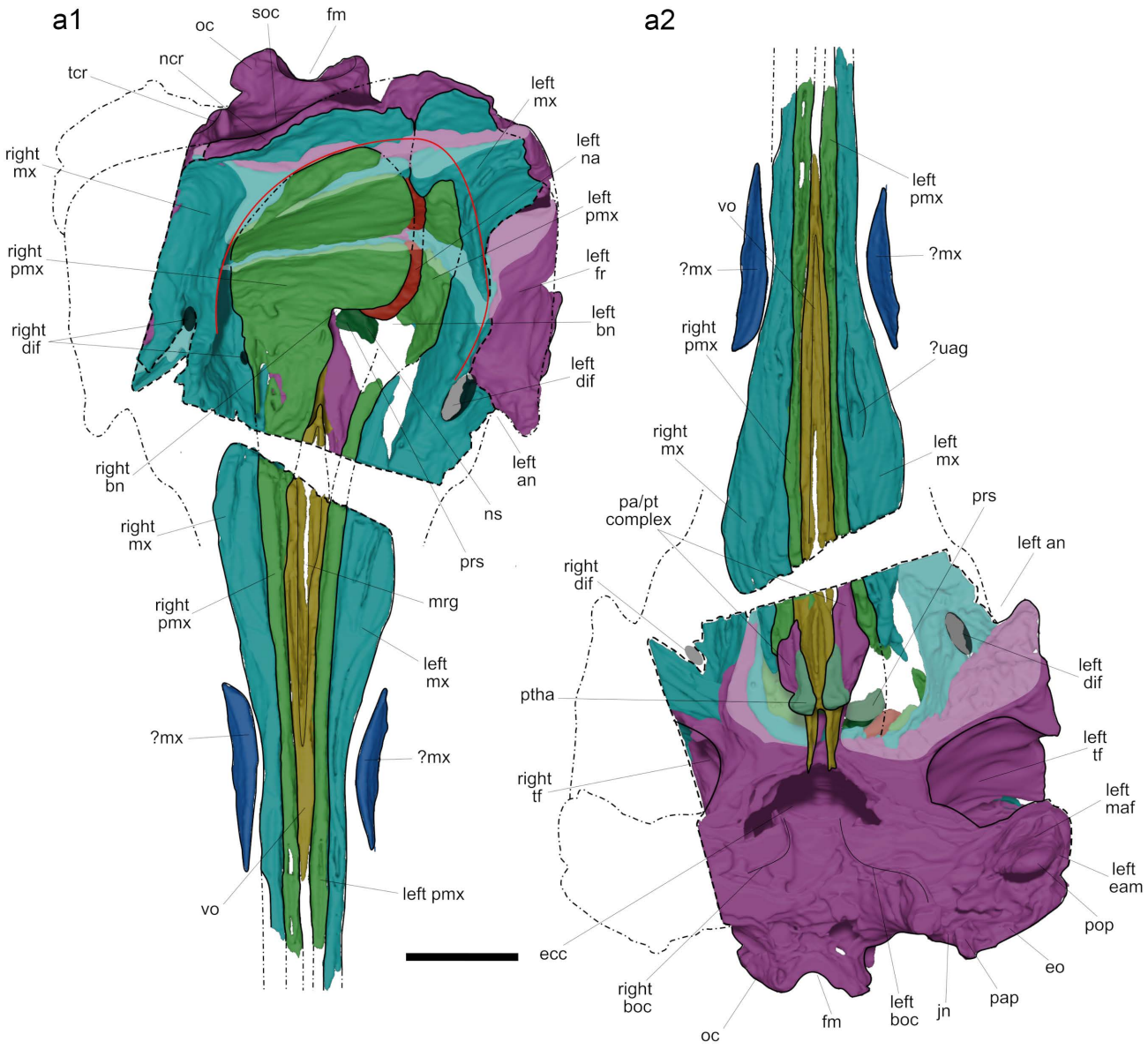

Fig. 4 - Retrodeformed 3D model of the cranium, in dorsal (a1) and ventral (a2) views, of *Angelocetus cursiensis* n. gen. n. sp. (MSNUP I-16954, holotype) from the Burdigalian (Lower Miocene) of the Pietra leccese. The grey-shaded areas indicate the presence of foramina. The white-shaded areas indicate cut surfaces on the neurocranium. The dash-dotted lines indicate reconstructed bone margins. The stippled lines indicate broken/eroded margins. The red line indicates the preserved margins of the supracranial basin. Scale bar equals 100 mm. An: antorbital notch; boc: basioccipital crest; bn: bony naris; dif: dorsal infraorbital foramen; eam: external auditory meatus; ecc: endocranial cavity; eo: esoccipital; fm: foramen magnum; fr: frontal; jn: jugular notch; maf: mandibular fossa; mrg: mesorostral groove; mx: maxilla; na: nasal; ncr: nuchal crest; ns: nasal septum; oc: occipital condyle; pa/pt: palatine-pterygoid; pap: paroccipital process; pmx: premaxilla; pop: postglenoid process; prs: presphenoid; ptha: pterygoid hamuli; soc: supraoccipital; tcr: temporal crest; tf: temporal fossa; uag: upper alveolar groove; vo: vomer. Light blue: maxilla; light green: premaxilla; yellow: vomer; dark green: presphenoid; red: left nasal; aquamarine: pterygoid; pink: neurocranium.

Kellogg, 1925, *M. chitaensis* and *O. crocodilinus*. This contrasts with the condition observed in *Thalassocetus* sp. (IRSNB M.2329), in which this margin is weakly concave. The osteoanatomy of *A. cursiensis* n. gen. n. sp. also differs from that observed in Kogiidae, in which a sagittal facial crest is present, and the medial margin of the right premaxilla is often sigmoid. The suture between the right premaxilla and the presphenoid is poorly defined. The right premaxilla/vomer suture is barely preserved at the base of the rostrum, whereas it becomes clearer toward the tip of the rostrum; it is rectilinear and runs parallel to the long axis of the rostrum.

The left premaxilla is more poorly preserved than the right, part of this bone being missing on the floor of supracranial basin. Posterior to the left bony naris, the left premaxilla rises posterodorsally to form the ascending process, which appears as a transversely narrow bony element. Along with the medial portion of the left maxilla, the ascending process of the left premaxilla contributes to form part of the left posterolateral wall of the supracranial basin. There, the lateral margin of the left premaxilla is higher than the adjacent margin of the left maxilla, forming an evident step-like structure. Posterodorsally, the ascending process of the left premaxilla exhibits a roughly

square-shaped termination. In this respect, *A. cursiensis* n. gen. n. sp. differs from *O. crocodilinus* USNM 14730 and from *Thalassocetus* sp. IRSNB M.2329, in which the posterodorsal end of the left premaxilla is falciform in shape. *Angelocetus cursiensis* n. gen. n. sp. also differs from O. *crocodilinus* USNM 22926 in having a higher and straighter lateral margin of the ascending process of the left premaxilla (the corresponding margin is almost semicircular in USNM 22926).

In ventral view, both the premaxillae appear as exposed throughout the anteroposterior length of the rostrum, delimiting laterally the vomer. Such an elongated ventral exposure of the premaxillae is unusual and likely resulted from the partial loss of the palatal processes of the maxillae due to pre-burial erosion.

Maxilla

In dorsal view (Figs 2, 4a1), the rostral portions of the maxillae display concave lateral margins. These concave margins are due to the tapered shape of the rostrum: in the anteriormost preserved 23 cm of the rostrum the maxillae are transversely narrow, and their lateral margins are straight and parallel to the main axis of the cranium, whereas more posteriorly the maxillae widen gradually, so that their lateral margins diverge progressively. Such a shape of the rostrum and maxillae somewhat recalls the condition observed in *Cozzuoliphyseter rionegrensis*, *Diaphorocetus poucheti* and *Koristocetus pescei*. In this respect, *Angelocetus cursiensis* n. gen. n. sp. differs from the macroraptorial physeteroids *Livyatan melvillei* and *Zygophyseter varolai*, in which the lateral margins of the maxillae are substantially straight along the rostrum. On the anteriormost slab entombing the rostrum, two elongated and laterally concave bony elements are discernible lateral to the preserved lateral margins of the maxillae. These elements do not contact the rostrum, and they were not included in the segmentation of the maxillae based on the CT images. However, given their position along both sides of the rostrum, these bony fragments may represent dislocated parts of the maxillae or, alternatively, portions of the mandibles.

Lateral to the supracranial basin, the dorsal surface of the partially preserved ascending process of the right maxilla is pierced by a large, slightly elliptical, 23-mm-wide dorsal infraorbital foramen that is abraded at its anterior margin. It is placed at the anterior end of a shallow, broad groove in the maxilla (transverse width about 19 mm) that is gently bent laterally. Medial to this groove, the right maxilla slightly rises in occurrence of the sharp, everted right lateral margin of the supracranial basin. The latter overhangs the gently concave right lateral wall of the supracranial basin. Whether this peculiar morphology is exaggerated by the post-burial deformation affecting the skull is uncertain. On the floor of the supracranial basin, the medial margin of the right maxilla is pierced by another sub-rectangular dorsal infraorbital foramen measuring 25 mm in anteroposterior length and 15 mm in transversal width. Such a partially preserved dorsal infraorbital foramen borders medially the lateral margin of the right premaxilla. On the 3D model, this foramen appears as having a circular shape. However, it should be noted that some relatively minor anatomical features such as foramina could display a slightly different morphology on the CT images due to the low contrast between the fossil bones and the entombing limestone and to the locally poor preservation state of the specimen. Differing from *Cozzuoliphyseter rionegrensis* and *Orycterocetus crocodilinus*, the portion of the right maxilla forming the lateral margin of the supracranial basin is not pierced by any dorsal infraorbital foramina. Posterolateral to the supracranial basin, the dorsal surface of the right maxilla exhibits a distinct transverse concavity and becomes almost vertical as it approaches the nuchal crest. The posterodorsal margin of the right maxilla is largely eroded. The incomplete ascending process of the right maxilla was probably wider transversely than that of its left antimere. The left dorsal infraorbital foramen, located medial to and at the same anteroposterior level as the antorbital notch, is oval and anteromedially elongated, measuring 45 mm in length and 16 mm in width. This foramen is followed posteriorly by a low ridge that contributes to define the left lateral margin of the supracranial basin. Remarkably, this margin appears as significantly lower than the right one, both on the original specimen and on the retrodeformed model, thus contributing to the overall asymmetry of the supracranial basin. In the retrodeformed 3D model, this part of the left maxilla gently slopes anteriorly to become almost vertical in its posteriormost portion. Lateral and posterolateral to this foramen, outside the supracranial basin, a large portion of the left maxilla is missing, thus exposing the underlying frontal. What remains of this portion of the left maxilla progressively rises posteromedially (average inclination 23° on the original specimen, 30° in the retrodeformed model). In occurrence of the posterior end of the left premaxilla, the medial margin of the left maxilla displays a thick ridge that is roughly dorsoventrally oriented. The posterior end of the left maxilla barely contacts the right maxilla and its dorsal surface is gently concave transversely; however, the poor preservation of this region of the cranium does not allow for ascertaining whether the right maxilla did originally reach the nuchal crest. In the original specimen, in lateral view (Fig. 3a4), the right maxilla slopes on the neurocranium to form an angle of about 17° with the horizontal plane. In the digital retrodeformed model (Fig. 5a2), the same angle is steeper, measuring 25°.

In ventral view, as reported above, the palatal surface of the maxillae appears as severely abraded due to pre-burial erosion, thus exposing large portions of the overlying premaxillae. Due to this damage, there is no unambiguous evidence of individual dental alveoli on the ventral surface of the maxillae. However, a deep and anteroposteriorly elongated sulcus takes its place along the left maxilla, being clear in CT images detailing the ventral aspect of the rostrum at mid-length. This sulcus can be tentatively interpreted as representing a remnant of an eroded alveolar groove. Whether this structure was functional (i.e., hosting erupted teeth) or vestigial (i.e., edentulous) is at present uncertain. Alternatively, considering the medial position of this deep and elongated sulcus, it may represent an anterior branch of the infraorbital canal.

Vomer

The vomer of *Angelocetus cursiensis* n. gen. n. sp. is only partially preserved: it lacks most of its dorsal

portion, except for two small fragments that are visible at the base of the rostrum and at the rostrum mid-length, respectively (Fig. 2). In dorsal view (Figs 2 and 4a1), the vomer forms the lateral walls of the mesorostral groove that starts anterolateral to the right bony naris. A similar condition also occurs in *Cozzuoliphyseter rionegrensis* and *Rhaphicetus valenciae*; differently, in *Acrophyseter* spp., *Orycterocetus crocodilinus* and *Zygophyseter varolai*, the mesorostral groove is anteroposteriorly aligned with the right bony naris. The transverse section of the preserved portion of the vomer is distinctly V-shaped for its whole length like in *Eudelphis mortzelensis, Placoziphius duboisi* and *Pliokogia apenninica*. This differs from the condition observed in *O. crocodilinus*, in which the dorsal surface of the vomer is U-shaped in transverse section. Both in the original specimen and in the CT images, a bony fragment, located slightly anterior to the antorbital notch, is here interpreted as the posterior end of the dorsal exposure of the vomer. In ventral view (Fig. 4a2), the vomer is visible along most of the preserved rostrum length, reaching a maximum breadth of about 3 cm. Such a ventral exposure of the vomer may be at least partially due to the erosion of the maxillae. The vomer is wedge-like and displays an acutely triangular anterior termination. Seemingly differing from *Livyatan melvillei* and several kogiids, the vomer does not appear to reach the anterior tip of the rostrum. Ventral to the region of the supracranial basin, the CT images shows two anteroposteriorly elongated bony laminae, which have been interpreted as part of the vomer. Moving ventrally, these elements converge to form an evident, anteroposteriorly elongated medial carina.

Presphenoid

The presphenoid is displaced toward the left side of the skull, being mostly covered by the right premaxilla and the single nasal. As in all other physeteroids, this bone is clearly asymmetric, and the keel of the nasal septum is tilted leftwards. The presphenoid forms the ventromedial floor of the right bony naris.

Nasal

Part of the posterior portion of the supracranial basin, between the right and the left maxilla, is comprised of a long, 20-mm-wide band of bone whose thickness ranges from a few millimetres to ca. 10 mm. This bony element, whose exact limits are difficult to define both in the original specimen and in the retrodeformed model, is here interpreted as the left nasal bone. This is the common condition for the physeteroids, two nasals being only observed in *Acrophyseter robustus* and *Miophyseter chitaensis*. The anteroventral margin of the nasal of *Angelocetus cursiensis* n. gen. n. sp. contacts the presphenoid. From there, the nasal rises posterodorsally, paralleling the medial margin of the right premaxilla; with its medially bowed shape, it recalls the condition observed in *Orycterocetus crocodilinus* and in the left nasal of *A. robustus*. The CT images reveal that the nasal is partly overlapped by the right premaxilla and partly overlaps the left premaxilla. Dorsally, in occurrence of a thick ridge of the left maxilla, the left nasal becomes thinner, and its dorsal termination almost reaches the dorsalmost slab cut.

Palatine-pterygoid complex

Entombed in the rock matrix, the suture between the pterygoid and the palatine is difficult to discern in the CT images. In ventral view, the lateral portion of the palatine-pterygoid complex (to be probably referred to the palatine) seemingly borders the posteriormost preserved portion of the premaxilla. This somewhat anomalous contact is likely due to the pervasive erosion of the ventral margin of the maxilla as well as to a significant degree of post-burial compression. The anterior margin of the palatines cannot be clearly discerned. Posterior to the level of the left antorbital notch, the palatine-pterygoid complex expands transversely. Posterolateral to the carina formed by the vomer, the hamular processes of the pterygoids take their place. These structures are posteriorly projected and laterally expanded, thus recalling the condition observed in the living sperm whale *Physeter macrocephalus*, in which the pterygoid hamuli display a transverse posterior widening.

Frontal

In left lateral view (Fig. 5a2), the retrodefomed model displays the dorsal surface of the supraorbital process of the frontal forming an angle of about 19° with the horizontal plane. Neither the left nor the right orbit are preserved. The wide portion of the frontal exposed beneath the missing parts of the ascending process of the left maxilla displays an abraded dorsal surface. This part of the frontal regularly rises posteriorly to become almost vertical approaching the nuchal crest. In dorsal view, a small and abraded portion of the frontal is seemingly observable posterodorsal to the posterior border of the ascending process of the left maxilla.

Squamosal

The supramastoid crest gently rises posteromedially. The area of the temporal fossa that in other physeteroids corresponds to the squamosal plate appears as concave and anteroventrolaterally elongated, recalling the morphology detected in *Diphorocetus poucheti* and *Orycterocetus crocodilinus*. *Angelocetus cursiensis* n. gen. n. sp. thus differs from *Acrophyseter deinodon*, in which the squamosal plate is slightly bulging. Anteromedial to the preserved part of the supramastoid crest, the squamosal displays a wide and deeply concave squamosal fossa, somewhat recalling Physeteroidea indet. MSNUP I-17076 but differing from *D. poucheti*, in which the squamosal fossa is shallower and more poorly defined. A thin, steep subtemporal crest limits the squamosal fossa anteroventrally. The zygomatic process of the squamosal is missing on both sides of the cranium, except for its very base that is preserved on the left squamosal (Fig. 5a2). The gently concave mandibular fossa faces anteroventromedially. Ventral to the mandibular fossa, a well-developed, anteroposteriorly thick postglenoid process distinctly projects ventrally. In the retrodeformed 3D model, the postglenoid process is remarkably elongated below the dorsoventral level of the posttympanic process. This condition differs from that of many crown physeteroids (e.g., *D. poucheti*, *O. crocodilinus*, *Physeter macrocephalus*, *Placoziphius duboisi* and *Thalassocetus antwerpiensis*) and the stem sperm whale *C. rionegrensis* as well, which exhibit a postglenoid process that is

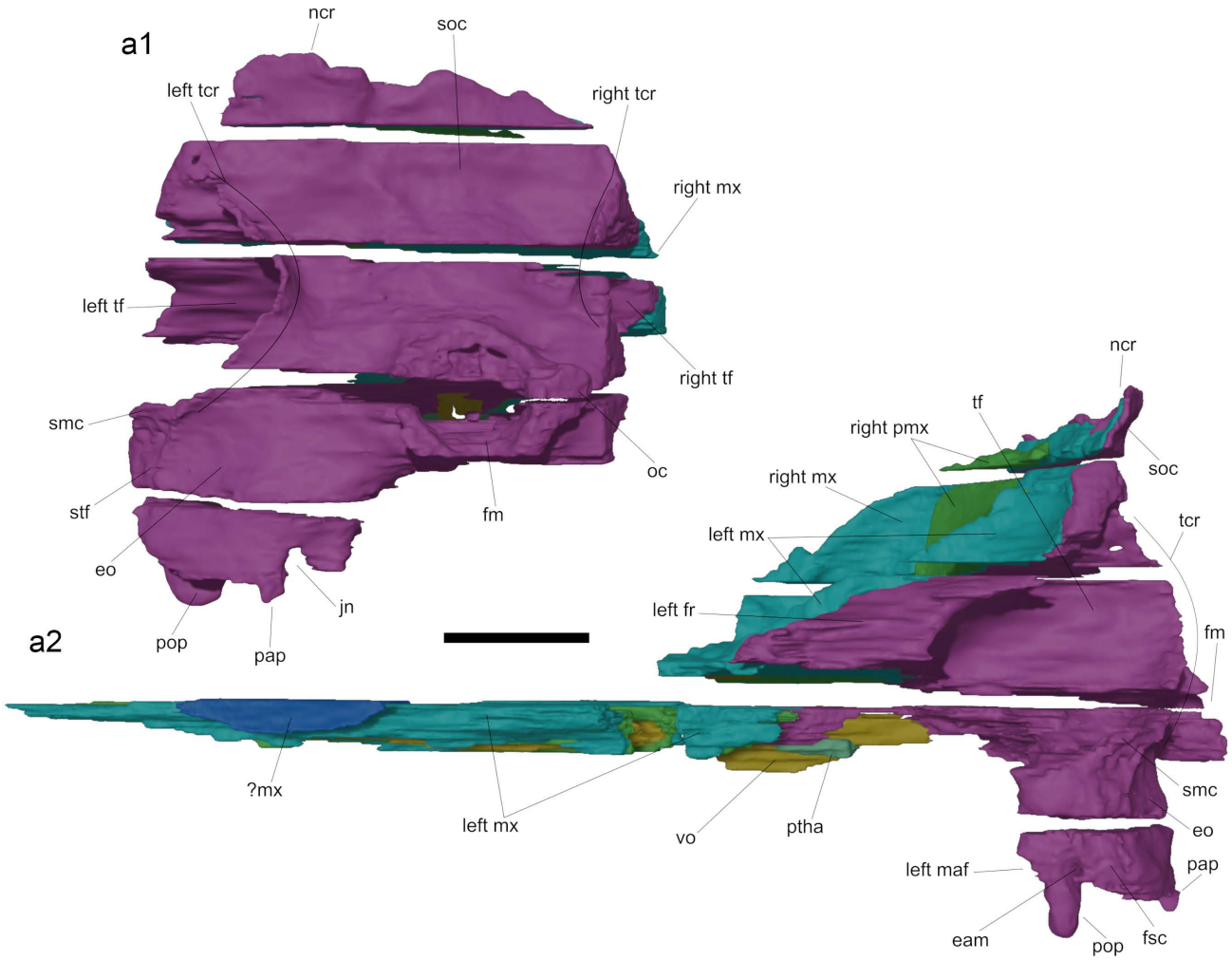

Fig. 5 - Retrodeformed 3D model of the cranium, in posterior (a1) and lateral (a2) views, of *Angelocetus cursiensis* n. gen. n. sp. (MSNUP I-16954, holotype) from the Burdigalian (Lower Miocene) of the Pietra leccese. Scale bar equals 100 mm. Eam: external auditory meatus; eo: esoccipital; fm: foramen magnum; fr: frontal; fsc: fossa for the sternocephalicus; jn: jugular notch; maf: mandibular fossa; mx: maxilla; ncr: nuchal crest; oc: occipital condyle; pap: paroccipital process; pmx: premaxilla; pop: postglenoid process; ptha: pterygoid hamuli; soc: supraoccipital; tcr: temporal crest; tf: temporal fossa; vo: vomer. Light blue: maxilla; light green: premaxilla; yellow: vomer; dark green: presphenoid; red: left nasal; aquamarine: pterygoid; pink: neurocranium.

less developed ventrally than the postympanic process. Posterior to the postglenoid process, the external auditory meatus is well discernible in ventral (Fig. 4a2) and lateral (Fig. 5a2) views. Posterior to the external auditory meatus, the posterolateral surface of the squamosal is excavated by a shallow, dorsoventrally elongated fossa for the sternocephalicus, recalling the condition detected in many other physeteroids (e.g., *Eudelphis mortezelensis*, *O. crocodilinus*, *Thalassocetus* sp. and *Zygophyseter varolai*). This condition differs from that observed in *Acrophyseter* spp. and in *Physeterula dubusi*, in which two distinct fossae are present. Posterior to this fossa, an anterolaterally bowed ridge that reaches the temporal crest marks the lateral margin of the exoccipital.

Supraoccipital

In the retrodeformed model, in left lateral view (Fig. 5a2), the occipital shield is almost vertically oriented. The supraoccipital is transversely wide and displays an evident asymmetry at its top. Such a posterior aspect of the supraoccipital crest is mainly due to the local abrasion of the nuchal crest that appears as sloping toward the right side of the skull.

Exoccipital

In posterior view (Fig. 5a1), the foramen magnum is roughly elliptical and depressed on the original specimen. As this structure has been used as reference for the subsequent retrodeformation, the foramen magnum appears as almost perfectly circular on the retrodeformed model. Regardless of the issues of retrodeformation, the shape of the foramen magnum of *Angelocetus cursiensis* n. gen. n. sp. differs from that of e.g., *Acrophyseter robustus* and *Kogia breviceps*, in which the foramen magnum displays a dorsal notch. Lateral to the foramen magnum, the best preserved right occipital condyle is somewhat reniform; like in *Acrophyseter deinodon*, *A. robustus*, *Orycterocetus crocodilinus* (USNM 14730) and *Physeter macrocephalus*, a constricted neck separates the occipital condyle from the rest of the neurocranium. Lateral to the occipital condyle, the exoccipital is a flaring, relatively high bony plate (a morphology that is

common to many other physeteroids). The ventral border of the exoccipital is expanded ventrolaterally to form the paroccipital process. The paroccipital process is oriented posteromedially and exhibits a roughly rectangular shape. This condition recalls that observed in *O. crocodilinus* but differs from that proper of *Diaphorocetus poucheti*, in which the paroccipital process is triangular. Medial to the paroccipital process, the ventral margin of the neurocranium is deeply incised by a wide, angular jugular notch that opens ventrally, thus differing from the holotype of *A. deinodon* (in which the jugular notch is ventrally closed and transformed into a true foramen by a medial expansion of the paroccipital process) but recalling *Eudelphis motzelensis*, *O. crocodilinus*, *Zygophyseter varolai* and Physeteroidea indet. MSNUP I-17076. *Angelocetus cursiensis* n. gen. n. sp. also differs from *Cozzuoliphyseter rionegresis*, which displays a narrow and partially closed jugular notch.

Basioccipital

In ventral view (Fig. 4a2), the preserved basioccipital exhibits a roughly trapezoidal shape that is transversely wider than anteroposteriorly long. The basioccipital crests delimiting the short basioccipital basin are partly preserved: the right one is mostly lost, except for its anteriormost portion, while the left is only locally damaged. The basioccipital crests significantly diverge and thicken backwards; a similar morphology is shared with many other physeteroids.

Mandible

Only a fragment of the right mandible, including the mandibular condyle, is preserved (Fig. 6). Considering the overall morphology of this mandible fragment and the position of the mandibular condyle, this bone piece likely belongs to the right dentary. This fragmentary mandible is located under the neurocranium, forming an angle of 43° with the axis of the rostrum; consequently, it was studied on the basis of the CT images only. In lateral view (Fig. 6a1), the coronoid process is subangular, recalling that of *Acrophyseter deinodon*. The mandibular condyle takes its place along the posterior margin of the mandible, posterodorsal to the angular process; it is posteriorly oriented, convex, and slightly prominent. Such a morphology differs from that observed in *Acrophyseter* spp., in which the condyle is posterodorsally directed and less protruding from the mandible outline, and in *Zygophyseter varolai*, in which the mandibular condyle is more posteriorly prominent. Ventromedially, the condyle displays a slight expansion that likely formed an insertion area for the masseter muscle. A reduced angular process is present in the form of an angular crest that protrudes at the posteroventral corner of the mandible, being located anteroventral to the mandibular condyle. In medial view (Fig. 6a2), the ventral margin of the mandibular foramen is partially preserved. This margin appears as gently curved; it runs posteriorly and slightly ventrally to form an angle of about 9° with the horizontal plane.

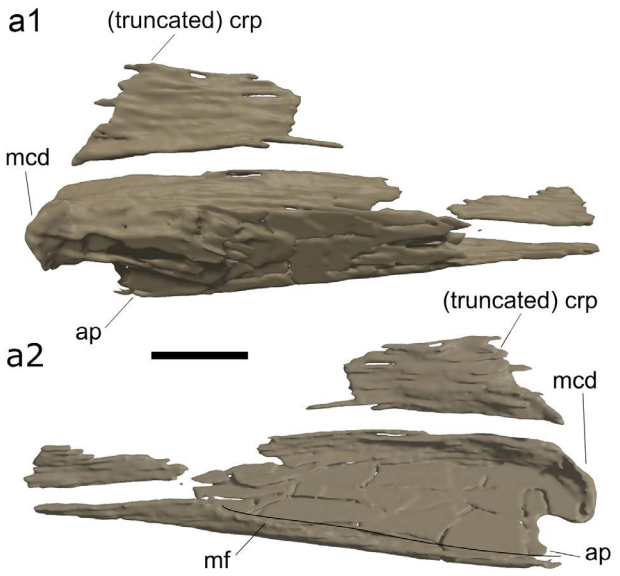

Fig. 6 - Right mandibular fragment, in lateral (a1) and medial (a2) views, of *Angelocetus cursiensis* n. gen. n. sp. (MSNUP I-16954, holotype) from the Burdigalian (Lower Miocene) of the Pietra leccese. Scale bar equals 50 mm. Ap: angular process; crp: coronoid process; mcd: mandibular condyle; mf: mandibular foramen.

Teeth

The holotype of *Angelocetus cursiensis* n. gen. n. sp. includes five fully prepared teeth, plus two teeth that are still embedded within the limestone matrix and were only imaged through the CT-scan. Measurements of the preserved teeth are provided in Table 1. All the preserved teeth are detached from their respective dental alveoli and their state of preservation is good (Fig. 7), except for one tooth in which parts of the root and crown were destroyed by the saw-cutting of the slabs (Fig. 7b1-3). The teeth of *A. cursiensis* n. gen. n. sp. are slender, fusiform and range in morphology from weakly curved to almost straight (Fig. 7). The general morphology of these teeth recalls that observed in *Rhaphicetus valenciae*, including slender teeth that are weakly curved or straight and bear and an enamelled crown. This contrasts with the condition observed in several derived physeteroids, including *Orycterocetus crocodilinus*, *Physeterula dubusi* and the extant genera *Kogia* and *Phsyeter*, which lack enamel (in adulthood at least). Furthermore, the teeth of *A. cursiensis* generally display a less pronounced curvature than observed in dental remains of *O. crocodilinus*. In addition, the teeth of *A. cursiensis* n. gen. n. sp. (average total length 84.6 mm, average maximum transverse width 17.1 mm) are larger than those of *O. crocodilinus* (average total length 54.6 mm, average maximum transverse width 8.9 mm) and *Diaphorocetus poucheti* (maximum width 10.3 mm).

The enamelled crown is conical, with a roughly circular transverse section. The ratio between the crown height (measured on teeth that display a low degree of apical wear) and the total tooth height ranges between 0.15 and 0.21. This ratio is smaller than that observed in Physeteroidea indet. MSNUP I-17076 (0.22-0.23), higher than in *Livyatan melvillei* (0.10-0.11), and close to *Zygophyseter varolai* (0.18). The enamel layer is thin (ca. 0.5 mm thick), and its surface is smooth; the crown-root transition is clear, without interdigitations. In this respect, *A. cursiensis* n. gen. n. sp. recalls *Myophyseter chitaensis* and *R. valenciae*, but differs from both Physeteroidea indet. MSNUP I-17076 and *Z. varolai*, which display an

Fig. 7 - Four detached teeth of *Angelocetus cursiensis* n. gen. n. sp. (MSNUP I-16954, holotype) from the Burdigalian (Lower Miocene) of the Pietra leccese in lingual/labial (a1, a3, b1, b3, c1, c3, d1, d3) and distal (a2, b2, c2, d2) views. The solid line indicates the outline of the pulp cavity. The stippled lines indicate the gingival collar. The arrows indicate the crown-root transition. Scale bar equals 50 mm.

ornamented enamel surface and interdigitations between the enamelled crown and the root. One tooth (Fig. 7c1-3) exhibits a distinct tapering of the root close to the interface with the crown; this feature is interpreted as the result of differential wear between the hard enamelled crown and the more delicate dentine of the root during food intake. A similar wear pattern has been detected in other sperm whale fossils like the holotype of *Acrophyseter robustus*, in some Late Miocene sperm whale teeth from Cessaniti (southern Italy) and in three physeteroid teeth from the Middle/Late Miocene of Groß Pampau (northern Germany) assigned by Hampe (2006) to *Hoplocetus ritzi* (Lambert et al., 2014, 2017; Marra et al., 2016).

The teeth are conic or fusiform (Fig. 7), exhibiting their maximum transverse width either at mid-height or more proximally (Fig. 7). This condition is similar to that observed in Physeteroidea indet. MSNUP I-17076, but it differs from that proper of *Z. varolai* and *Acrophyseter* spp., in which the tooth roots display their maximum diameter close to the base of the crown. The transverse section of the teeth is slightly elliptical except for one tooth that displays a peculiar trapezoidal section (Fig. 7c1-3). The roots are slender (ratio between the maximum transverse root diameter and height ranging between 0.19 and 0.23) if compared to Physeteroidea indet. MSNUP I-17076 (0.23-0.30), *Acrophyseter* sp. MUSM 2182 (0.27-0.38) and *Z. varolai* (0.31-0.35). As for the adult individuals of the extant physeteroid genera (*Physeter* and *Kogia*), *O. crocodilinus* and the holotype of *Scaldicetus caretti* (Boschma, 1938; Lambert & Bianucci, 2019), the teeth of *A. cursiensis* n. gen. n. sp. exhibit an open pulp cavity (Fig. 7b1). The pulp cavities of *A. cursiensis* reach a maximum transverse width of about 10 mm and displays a rounded roof, thus differing from the pointed roof observed in the holotype of *S. caretti*. In Physeteroidea indet. MSNUP I-17076, *Z. varolai* and *Acrophyseter* spp. the pulp cavity is in turn filled by dentine and closed. The root surface of some teeth (Fig. 7b2-3, c1-3) is partially coated by a thin layer of dark material. In other fossil physeteroids, this dental feature was named "gingival collar" and interpreted as the contact area between the gum and the tooth (Bianucci & Landini, 2006; Lambert et al., 2008, 2014, 2017). Such a coating may represent the calculus (i.e., dental plague) deposited between the gum and the tooth, as observed by Lambert & Bianucci (2019) on the type material of *S. caretti* and by Loch et al. (2011) in extant toothed whales. As in *Z. varolai*, the gingival collar appears as a narrow band, ca. 4 mm in dorsoventral height. From the orientation of the preserved gingival collars, it may be inferred that the anatomical inclination of some preserved teeth with the horizontal plane was about 65°. Assuming that the root sides that display an obliquely oriented gingival collar were facing either labially or lingually, a remarkable degree of labiolingual compression is observed in one of the preserved teeth (Fig. 7c1-3). A labiolingual compression of the root is also observed in the posterior lower teeth of *Acrophyseter deinodon* and *Z. varolai* (Bianucci & Landini, 2006; Lambert et al., 2008, 2017; Peri et al., 2021). Two teeth display a very limited degree of apical wear (Fig. 7a1-2, d1-3), with only few millimetres of crown height being lost, while the apical

	1	2	3	4	5	6	7
Total length	92.5	94.9	72.4	91*	98.9	**56.6***	**64.4**
Root length	74.1	85.5	59.3	80.4*	87.9	**56.6***	**54.7**
Crown length	19	11	13.1	11.2*	15.2	**NA**	**9.4**
Maximum labiolingual diameter of root	13.9*	14.2	12.8	11.7*	NA	**NA**	**NA**
Maximum mesiodistal diameter of root	17.1	17.3	13.5	18.4	19.1	**NA**	**12.3***
Transverse diameter at crown base	9.5	9.2	7.7	6.8*	NA	**NA**	**NA**
Mesiodistal diameter at crown base	10	8.6	7.8	9.5	9.6	**NA**	**10.4***

Tab. 1 - Measurements of detached teeth of of *Angelocetus cursiensis* n. gen. n. sp. (MSNUP I-16954, holotype) from the Burdigalian (Lower Miocene) of the Pietra leccese. Note that the tooth numbering used here does not reflect the anatomical position of the teeth. The measures of the detached teeth observed in the CT images are reported in bold. All measurements are reported in millimetres. *: incomplete measure; NA: not available.

wear on another tooth is slightly more pronounced (Fig. 7c1-3). No occlusal wear surfaces were detected in any of the preserved teeth.

PHYLOGENY

Our phylogenetic analysis produced 3240 most parsimonious trees having a tree length of 166, a Consistency Index (CI) of 0.473, and a Retention Index (RI) of 0.713. The most parsimonious trees are summarized in a strict consensus tree that is shown in Figure 8, as well as in a 50% majority rule consensus tree provided in the Fig. S1 of the SOM 3. The bootstrap analysis produced generally low values, and only few nodes appear as well supported. This may reflect the fragmentary nature of some of the taxa included in the present analysis. The poor preservation state of MUSM 2182 (*Acrophyseter* sp.) is likely reflected in the relationship with the genus *Acrophyseter* Lambert et al., 2008 being polytomic; thus, this genus was collapsed. Moreover, considering that the resolution of intra-Kogiidae phylogenetic relationships is beyond the aim of the present paper, kogiids were also graphically collapsed.

The base of Physeteroidea is marked by a polytomy involving: 1) the Early-Middle Miocene species *Eudelphis mortezelensis*; 2) the Early Miocene species *Rhaphicetus valenciae*; 3) a monophyletic group, here informally referred to as the "*Zygophyseter*-clade", which is comprised of three Miocene genera of macroraptorial sperm whales (i.e., *Acrophyseter*, *Brygmophyseter* Barnes in Kimura et al., 2006 and *Zygophyseter* Bianucci & Landini, 2006); and 4) a clade formed by *Cozzuoliphyseter rionegrensis* plus the crown physeteroids, featuring many Early to Late Miocene genera (including the giant macroraptorial genus *Livyatan* Lambert et al., 2010) besides the extant families Kogiidae and Physeteridae. Here, the family Physeteridae is defined on a cladistic basis as the least inclusive clade comprising all the phsyeteroids that are more closely related to *Physeter macrocephalus* than to the extant *Kogia* spp. Kogiidae, in turn, is a highly autapomorphic family characterised by the presence of a sagittal facial crest. Notably, our phylogenetic analysis recovers the giant macroraptorial sperm whale *Livyatan melvillei* as sister group to the small-sized sperm whales that comprise the family Kogiidae. This peculiar positioning contrasts with those recovered by several previous studies in which *L. melvillei* was recovered as nested among the macroraptorial sperm whales (Collareta et al., 2017, 2019, 2020; Paolucci et al., 2020, 2021; Alfsen et al., 2021) or at the base of a clade including *C. rionegrensis* and the crown physeteroids (Lambert et al., 2017). That said, a "*Zygophyseter*-clade" including *Zygophyseter varolai*, *Acrophyseter* spp. and *Brygmophyseter shigensis* has been recognised by several phylogenetic reconstructions, though with the occasional addition of *L. melvillei* and *C. rionegrensis* (Collareta et al., 2017, 2019a, 2020; Lambert et al., 2017; Benites-Palomino et al., 2020; Paolucci et al., 2020, 2021; Alfsen et al., 2021; Kimura & Hasegawa, 2022).

According to our cladistic results, *A. cursiensis* n. gen. n. sp. belongs with the crown sperm whale clade and is nested within a wide polytomy that includes *Diaphorocetus poucheti*, *Placoziphius duboisi* and *Thalassocetus* spp., with *Orycterocetus crocodilinus* as sister group. In the 50% majority rule consensus tree (SOM 3, Fig. S1), the position of *A. cursiensis* n. gen. n. sp. is fully resolved, as it appears as the sister group of a clade formed by *D. poucheti* and *P. duboisi*. In the strict consensus tree, the clade including *A. cursiensis* n. gen. n. sp. and *O. crocodilinus* is sister group to a clade formed by *Miophyseter chitaensis* (also recovered as a crown physeteroid by Kimura & Hasegawa, 2022), *L. melvillei* and Kogiidae; thus, *A. cursiensis* n. gen. n. sp. appears as more closely related to *L. melvillei* and Kogiidae than to the physeterids. According to our results, the latter family is limited to the extant sperm whale (*Physeter macrocephalus*) and a few fossil forms (i.e., *Aulophyseter morricei*, *Idiophyseter merriami, Idiorophus patagonicus* [Lydekker, 1894] and *Physeterula dubusi*). This contrast with Alfsen et al. (2021) which recovered *D. poucheti*, *P. duboisi*, *Thalassocetus* spp. and *O. crocodilinus* as part of Physeteridae. A close relationship between the extant *P. macrocephalus* and *A. morricei*, *I. merriami* and *P. dubusi* was previously suggested in several investigations (Lambert et al., 2020; Paolucci et al., 2020, 2021; Alfsen et al., 2021; Kimura & Hasegawa, 2022).

Interestingly, the new character (c. 54) added by us with respect of the last published phylogeny of the physeteroids by Alfsen et al. (2021), shows that the lateral expansion of the supracranial basin occurred independently in three major sperm whale clades - i.e., the "*Zygophyseter*-clade", *L. melvillei* + Kogiidae, and Physeteridae. Once again, it is worth mentioning that the low bootstrap values, along with the numerous topological variations displayed by the phylogenetic trees presented in recent years, denote an instability in the phylogeny of sperm whales. This issue highlights the need of new studies to further explore the phylogenetic relationship across Physeteroidea, possibly via the inclusion of new characters in the current matrix.

DISCUSSION

The osteoanatomy of *Angelocetus cursiensis* n. gen. n. sp. provides some hints about its possible trophic strategy and diet. The observation of relatively small, slender teeth (somewhat recalling those of *Rhaphicetus valenciae* and *Miophyseter chitaensis*) featuring a thin and unornamented enamel layer coating the crown strongly contrasts with the dental morphology of those physeteroid species that are currently interpreted as macroraptorial feeders (i.e., *Acrophyseter* spp., *Brygmophyseter shigensis* [Hirota & Barnes, 1994], *Livyatan melvillei* and *Zygophyseter varolai*) (Bianucci & Landini, 2006; Kimura & Hasegawa, 2006; Lambert et al., 2008, 2010, 2014, 2017; Peri et al., 2020, 2021). That said, the presence of large and anteroposteriorly elongated temporal fossae separates *A. cursiensis* n. gen. n. sp. from the suction-feeding, mostly teuthophagous extant physeteroids *Physeter macrocephalus* and *Kogia* spp., characterised by a dorsoventrally low and anteroposteriorly short temporal fossa (Werth, 2004, 2006b; Bloodworth & Marshall, 2005; Staudinger et al., 2014). It is important to underline that the teuthophagous extant physeteroids also display another character related to the suction feeding behaviour:

the loss of functional upper teeth. Unfortunately, it is not possible to verify this character in *A. cursiensis* n. gen. n. sp. due to the incompleteness of the holotype and only known specimen. On the one hand, the apparent absence of occlusal wear facets in the *A. cursiensis* n. gen. n. sp. teeth may support the interpretation of a lack of functional upper dentition in the latter, though only seven teeth were recovered (five of which were fully prepared); on the other hand, the observation of a large temporal fossa suggests that this species was able to produce relatively powerful bites, which in extant odontocetes is associated with a raptorial feeding behaviour. The rostral index (ratio between the condylobasal length and the rostral length; McCurry & Pyenson, 2019) of *A. cursiensis* n. gen. n. sp. is at least 0.62; considering that this value is somewhat underestimated due to the lack of the anterior portion of the rostrum, this fossil physeteroid falls among the longirostrine forms as defined by McCurry & Pyenson (2019). Coupled with the aforementioned cranial and dental features, such an elongated rostrum suggests that *A. cursiensis* n. gen. n. sp. may have been a raptorial pierce feeder that captured its prey items by means of biting and then swallowed them whole with the aid of suction (Werth, 2006b; Kienle et al., 2017; Berta & Lanzetti, 2020). Remarkably, the masseter muscle, one of the most prominent mandibular adductors along with the temporal, may also play an important role in the nutrition of extant suction feeding physeteroids (Benites-Palomino et al., 2021). Similar to the condition observed in some specimens of *P. macrocephalus* and *Kogia breviceps*, the preserved mandibular fragment of *A. cursiensis* n. gen. n. sp. features a distinct angular process, representing the insertion area of the masseter muscle on the mandible. Therefore, the masseter was probably well developed in *A. cursiensis* n. gen. n. sp., possibly allowing for a rapid elevation of the mandibles. Considering the body size and the absolute size of its teeth, it is likely that *A. cursiensis* fed mainly on medium- and large-sized fishes. Interestingly, other living odontocetes known as pierce feeders (e.g., the river dolphins *Inia geoffrensis* Blainville, 1817 and *Platanista gangetica* Lebeck, 1801) display wide temporal fossae, small teeth and elongated rostra (McCurry & Pyenson, 2019; Berta & Lanzetti, 2020).

Among the taxa that are phylogenetically closer to *A. cursiensis* n. gen. n. sp., *Orycterocetus crocodilinus* may have used a similar pierce feeding strategy, based on the elongated rostrum (rostral index 0.58) having a bottlenecked outline, the presence of a functional upper dentition (testified by occlusal facets on teeth) and the slender tooth shape. However, the less elongated temporal fossa and the smaller teeth suggest some differences between the feeding strategies of *A. cursiensis* n. gen. n. sp. and *O. crocodilinus* (which likely reflects different target prey items). In turn, the cranial morphology of *Diaphorocetus poucheti* (featuring an elongated zygomatic process, narrow and deep upper alveoli that are separated by interalveolar septa, and laterally thin teeth) suggests a raptorial-like feeding strategy for this extinct sperm whale (Paolucci et al., 2020). Interestingly, in spite of the high diversity of physeteroids during the Burdigalian (Fig. 8), several sperm whales from this time span (*D. poucheti*, *Idiorophus patagonicus* and *Miophyseter chitaensis*) share with *A. cursiensis* n. gen. n. sp. a similar body size (body length values ranging between 3.5-5 m) as well as cranial and dental morphologies that are possibly related with a raptorial-like feeding strategy (including a temporal fossa that is relatively more developed than observed in the extant suction feeding genera *Physeter* and *Kogia*, a rostrum that is broad at its base and anteriorly narrow, the presence of a functional upper dentition, and thin and slender teeth) (Paolucci et al., 2020; Kimura & Hasegawa, 2022). The diffusion of these morphological features among the Burdigalian physeteroids suggest a low degree of trophic niche partitioning. An exception is represented by *Rhaphicetus valenciae*, which displays a peculiar rostral morphology as well as the occurrence of bony pads within the anteriormost upper dental alveoli, suggesting a unique feeding behaviour that may have involved grasping relatively small-sized prey items via rapid movements of the head (Lambert et al., 2020; Bianucci & Collareta, 2022). The subsequent Langhian epoch marks the appearance of the first macroraptorial physeteroids (*Brygmophyseter*; Kimura et al., 2006), some of which display a large body size (*Albicetus* Boersma & Pyenson, 2015), as well as that of the earliest sperm whales (*Aulophyseter morricei*) with specialised suction feeding traits (loss of functional upper teeth, reduction of the temporal fossa), resulting in a significant increase of the morphological disparity and ecological diversity within this important cetacean clade.

According to our results, *D. poucheti*, *Placoziphius duboisi* and *Thalassocetus* spp. are phylogenetically closest to *A. cursiensis* n. gen. n. sp. All the materials referred to these species was recovered from along the Northern and Southern Hemisphere coasts of the Atlantic Ocean (Van Beneden, 1869; Moreno, 1892; Abel, 1905; Lambert, 2008; Paolucci et al., 2020). Considering this, the phylogenetic relationships of *A. cursiensis* n. gen. n. sp. indicate some degree of biogeographic connectivity between the Mediterranean and Atlantic basins during the late Early Miocene. Interestingly, such a relationship was previously evoked by the discovery of an incomplete mandible of *Orycterocetus*, a typical component of the Early/Middle Miocene marine mammal assemblages of the Northern Atlantic, in deposits of the Pietra leccese exposed near Cursi (Bianucci et al., 2004).

CONCLUSIONS

We described a new sperm whale fossil from the Burdigalian (Lower Miocene) strata of the Pietra leccese formation of Apulia (southern Italy). As this specimen is only partially freed from the hard limestone matrix and displays a remarkable degree of dorsoventral compression, it was imaged by means of CT-scan. Both the segmentation of the CT images and the direct observation of the restored portions of the skull revealed that this fossil belongs to a new medium-sized genus and species (*Angelocetus cursiensis* n. gen. n. sp.) characterised by a posterolaterally directed asymmetry of the supracranial basin, as well as by a combination of cranial and dental features (e.g., an anteroposteriorly elongated temporal fossa, a ventrally developed postglenoid process, and enamelled tooth crowns) which, all together, distinguish this new taxon from all other closely related physeteroid species. To improve our understanding of the osteoanatomy of this fossil sperm

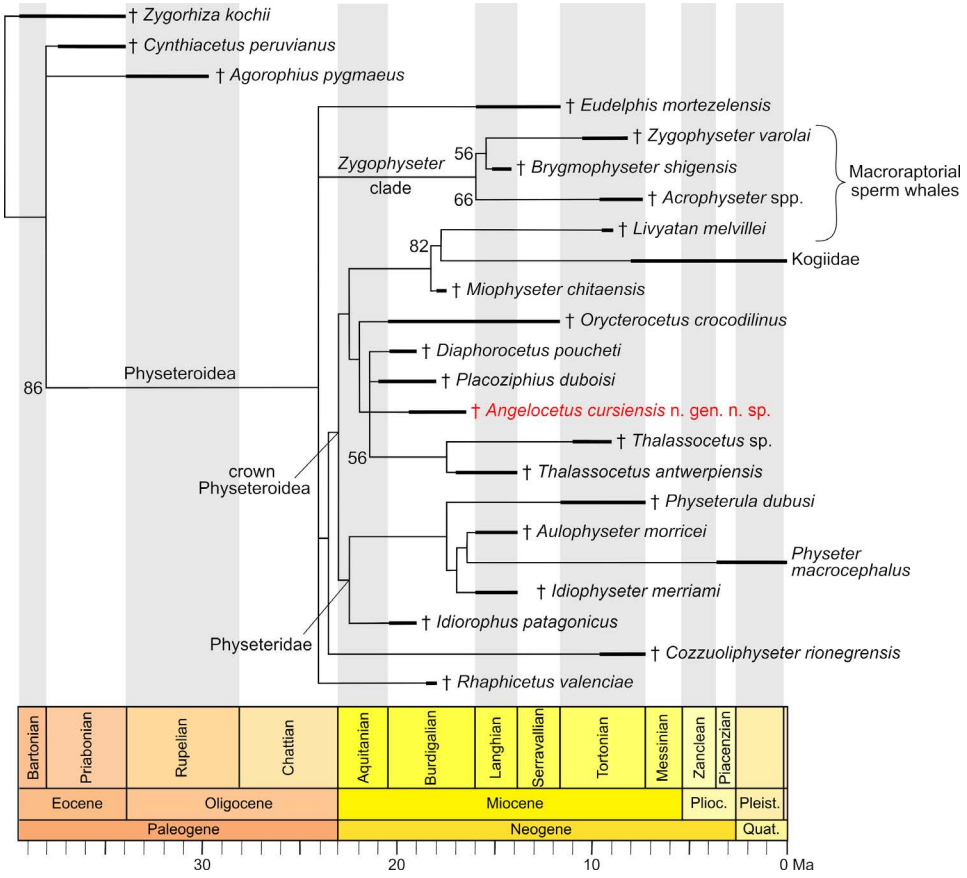

Fig. 8 - Time-calibrated strict consensus tree of 3240 most parsimonious trees having a tree length of 166, a consistency index (CI) 0.476 and a retention index (RI) 0.7166, describing the phylogenetic relationships of *Angelocetus cursiensis* n. gen. n. sp. (highlighted in red) among Physeteroidea. The strict consensus tree was obtained by the heuristic search of equal-weighted and unordered characters. Bootstrap values higher than 50 are indicated at nodes. The chronostratigraphic ranges of the included taxa are mostly from Paolucci et al. (2020); for *Rhaphicetus valenciae* and *Thalassocetus* sp. IRSNB M.2329 we followed Lambert et al. (2020) and Alfsen et al. (2021), respectively. The complete strict and 50% majority rule consensus trees are provided in the SOM 3.

whale we retrodeformed the 3D model obtained from the CT-scan by using the shape of the foramen magnum as a proxy. The retrodeformed model greatly enhanced the description of the specimen and strengthened the notion that the obvious eccentricity of the supracranial basin is a genuine diagnostic trait of *A. cursiensis* n. gen. n. sp. and not the result of post-burial taphonomic deformation. Our phylogenetic analysis recovers *A. cursiensis* n. gen. n. sp. as a crown physeteroid that does not belong to either of the extant physeteroid families. The relatively reduced body size, the presence of a well-developed temporal fossa, the elongated rostrum, and the slender teeth provided with a thin and unornamented enamel layer evoke a diet based on medium- and large-sized fish that were likely captured with a pierce feeding strategy. During the Burdigalian, a similar ecological niche was occupied by several other sperm whales, with the possible exclusion of *Rhapicetus valenciae*, which likely used to feed on relatively small-sized prey via rapid movements of the head. Despite such an apparent low ecomorphological disparity, the high degree of taxonomic diversity of the Burdigalian physeteroids (at least six species) suggests that this epoch represents a critical time span for the evolutionary history of the sperm whales. Moreover, the roughly coeval presence of basal (*R. valenciae*) and derived (crown-group) forms (*Angelocetus cursiensis* n. gen. n. sp., *Diaphorocetus poucheti*, *Idiorophus patagonicus*, *Miophyseter chitaensis* and *Placoziphius duboisi*) of sperm whales during the Burdigalian evokes the long-lasting persistence of ghost lineages, thus also indicating that the Miocene radiation of Physeteroidea is far from being fully understood. The new physeteroid species presented herein further expands the taxonomic diversity of the physeteroid fossil assemblage from the Pietra leccese formation. Finally, the phylogenetic relationships of *A. cursiensis* n. gen. n. sp. support the existence of a palaeobiogeographic connection between the Mediterranean Basin and the Atlantic Ocean during the late Early Miocene.

SUPPLEMENTARY ONLINE MATERIAL

Supplementary data of this work are available on the BSPI website at: https://www.paleoitalia.it/bollettino-spi/bspi-vol-612/

ACKNOWLEDGEMENTS

We are grateful to Fabrizio Cancelli, Letizia Del Favero, Simone Farina, Mariagabriella Fornasiero, Walter Landini, Olivier Lambert, Christine Lefèvre, Giuseppe Manganelli, James G. Mead, Christian de Muizon, Charles W. Potter, Nicholas D. Pyenson, Daniel Robineau, Rodolfo Salas Gismondi, Vincenzo Vomero and Chiara Sorbini, for providing access to specimens under their care and for fruitful discussions about several topics covered in this paper. We also thank the whole staff of the Diagnostic and Interventional Radiology unit of the Cisanello University Hospital for their expert technical support. Our gratitude also goes to Olivier Lambert and Aldo Benites-Palomino, for their constructive reviews, and to Giorgio Carnevale, for his expert editorial support.

REFERENCES

Abel O. (1905). Les Odontocètes du Boldérien (Miocène supérieur) des environs d'Anvers. III. *Mémoires du Musée Royal d'Histoire Naturelle de Belgique*, 3: 1-155.

Aldinio P. (1896). Sul *Tomistoma* (*Gavialosuchus*) *lyceensis* del calcare miocenico di Lecce. *Atti Dell'Accademia Gioenia Di Scienze Naturali Di Catania (Serie 4)*, 9: 1-11.

Alfsen A., Bosselaers M. & Lambert O. (2021). New sperm whale remains from the late Miocene of the North Sea and a revised family attribution for the small crown physeteroid *Thalassocetus* Abel, 1905. *Comptes Rendus Palevol*, 20: 807-822.

Ambrose S.T., Froneman P.W., Smale M.J., Cliff G. & Plön S. (2013). Winter diet shift of long-beaked common dolphins (*Delphinus capensis*) feeding in the sardine run off KwaZulu-Natal, South Africa. *Marine Biology*, 160: 1543-1561.

Balenzano F., Margiotta S. & Moresi M. (2002). Significato di un deposito glauconitico-fosfatico appartenente ad una Unità Miocenica del Salento (Puglia). *Atti della Società Toscana di Scienze Naturali, Memorie, Serie A*, 108: 7-21.

Balenzano F., Moresi M. & Tria A. (1994). Significato paleogeografico della presenza di Glauconite nella "Pietra leccese" (Calcarenite Miocenica del Salento). *Mineralogica et Petrographica Acta*, 37: 437-450.

Benites-Palomino A., Vélez-Juarbe J., Altamirano-Sierra A., Collareta A., Carrillo-Briceño J.D. & Urbina M. (2022). Sperm whales (Physeteroidea) from the Pisco Formation, Peru, and their trophic role as fat sources for late Miocene sharks. *Proceedings of the Royal Society B*, 289 (1977): 20220774.

Benites-Palomino A., Vélez-Juarbe J., Collareta A., Ochoa D., Altamirano A., Carré M., Laime M.J., Urbina M. & Salas-Gismondi R. (2021). Nasal compartmentalization in Kogiidae (Cetacea, Physeteroidea): insights from a new late Miocene dwarf sperm whale from the Pisco Formation. *Papers in Palaeontology*, 7: 1507-1524.

Benites-Palomino A., Vélez-Juarbe J., Salas-Gismondi R. & Urbina M. (2020). *Scaphokogia totajpe*, sp. nov., a new bulky-faced pygmy sperm whale (Kogiidae) from the late Miocene of Peru. *Journal of Vertebrate Paleontology*, 39: e1728538.

Berta A. & Lanzetti A. (2020). Feeding in marine mammals: An integration of evolution and ecology through time. *Palaeontologia Electronica*, 23: 1-42.

Bianucci G. (1996). I cetacei fossili del Museo di Storia Naturale dell'Università di Pisa. *Atti della Società Toscana di Scienze Naturali, Memorie, Serie A*, 103: 63-68.

Bianucci G. (2001). A new genus of kentriodontid (cetacea: Odontoceti) from the miocene of South Italy. *Journal of Vertebrate Paleontology*, 21: 573-577.

Bianucci G., & Collareta A. (2022). An overview of the fossil record of cetaceans from the East Pisco Basin (Peru). *Bollettino della Società Paleontologica Italiana*, 61: 19-60.

Bianucci G., Collareta A., Post K., Varola A. & Lambert O. (2016). A new record of *Messapicetus* from the Pietra Leccese (Late miocene, Southern Italy): Antitropical distribution in a fossil beaked whale (Cetacea, Ziphiidae). *Rivista Italiana di Paleontologia e Stratigrafia*, 122: 63-74.

Bianucci G. & Landini W. (2002). Change in diversity, ecological significance and biogeographical relationships of the Mediterranean Miocene toothed whale fauna. *Geobios* 35: 19-28.

Bianucci G. & Landini W. (2003). *Metaxytherium medium* (Mammalia: Sirenia) from upper Miocene sediments of the Arenaria di Ponsano Formation (Tuscany, Italy). *Rivista Italiana di Paleontologia e Stratigrafia*, 109: 567-573.

Bianucci G. & Landini W. (2006). Killer sperm whale: A new basal physeteroid (Mammalia, Cetacea) from the Late Miocene of Italy. *Zoological Journal of the Linnean Society*, 148: 103-131.

Bianucci G., Landini W. & Varola A. (1992). *Messapicetus longirostris*, a new genus and species of Ziphiidae (Cetacea) from the late Miocene of "Pietra leccese" (Apulia, Italy). *Bollettino della Società Paleontologica Italiana*, 31: 261-264.

Bianucci G., Landini W. & Varola A. (1994). New remains of Cetacea Odontoceti from the Pietra Leccese (Apulia, Italy). *Bollettino della Società Paleontologica Italiana*, 33: 231-242.

Bianucci G., Landini W. & Varola A. (2003). New records of *Metaxytherium* (Mammalia: Sirenia) from the late Miocene of Cisterna quarry (Apulia, southern Italy). *Bollettino della Società Paleontologica Italiana*, 42: 59-63.

Bianucci G., Landini W. & Varola A. (2004). First discovery of the Miocene northern Atlantic sperm whale *Orycterocetus* in the Mediterranean. *Geobios*, 37: 569-573.

Bianucci G. & Varola A. (1994). Kentriodontidae (Odontoceti, Cetacea) from Miocene sediments of the Pietra leccese (Apulia, Italy). *Atti della Società Toscana di Scienze Naturali, Memorie, Serie A*, 101: 201-212.

Bianucci G. & Varola A. (2014). I cetacei fossili della Pietra leccese nei musei del Salento. *Museologia Scientifica, Memorie*, 13: 130-134.

Bisconti M. (2008). Morphology and phylogenetic relationships of a new eschrichtiid genus (Cetacea: Mysticeti) from the Early Pliocene of northern Italy. *Zoological Journal of the Linnean Society*, 153: 161-186.

Bisconti M. & Varola A. (2006). The oldest eschrichtiid mysticete and a new morphological diagnosis of eschrichtiidae (Gray Whales). *Rivista Italiana di Paleontologia e Stratigrafia*, 112: 447-457.

Blainville H. de (1817). *In* Desmarest A.G. (ed.), Nouveau dictionnaire d'histoire naturelle. Vol. 9. 151 pp. Deterville, Paris.

Blainville H.M. de (1838). Sur les cachalots. *Annales Françaises et Étrangères d'Anatomie et de Physiologie*, 2: 335-337.

Bloodworth B. & Marshall C.D. (2005). Feeding kinematics of *Kogia* and *Tursiops* (Odontoceti: Cetacea): characterization of suction and ram feeding. *Journal of Experimental Biology*, 208: 3721-3730.

Boersma A.T. & Pyenson N.D. (2015). *Albicetus oxymycterus*, a new generic name and redescription of a basal physeteroid (Mammalia, Cetacea) from the Miocene of California, and the evolution of body size in sperm whales. *PLOS ONE*, 10: e0135551.

Boschma H. (1938). Double Teeth in the Sperm Whale (*Physeter macrocephalus* L.). *Zoologische Mededelingen*, 20: 211-221.

Bossio A., Foresi L.M., Margiotta S., Mazzei R., Salvatorini G. & Donia F. (2006). Stratigrafia neogenico-quaternaria del settore nord - Orientale della provincia di Lecce (con rilevamento geologico alla scala 1:25.000). *Geologica Romana*, 39: 63-87.

Bossio A., Mazzei R., Monteforti B. & Salvatorini G. (2005). Stratigrafia del Neogene e Quaternario del Salento sud-orientale (con rilevamento geologico alla scala 1: 25.000). *Geologica Romana*, 38: 31-60.

Calia A., Tabasso M.L., Mecchi A.M. & Quarta G. (2014). The study of stone for conservation purposes: Lecce stone (southern Italy). *Geological Society, London, Special Publications*, 391: 139-156.

Capellini G. (1878). Della Pietra Leccese e di alcuni suoi fossili. *Memorie della Accademia delle Scienze dell'Istituto di Bologna*, 3: 227-258

Capellini G. (1897). A proposito di *Tomistoma lyceensis*. *Rivista Italiana di Paleontologia*, 3: 18-20.

Carnevale G., Sorbini C., Landini W. & Varola A. (2002). *Makaira* cf. *M. nigricans* Lacepede, 1802 (Teleostei: Perciformes: Istiophoridae) from the Pietra Leccese, Late Miocene, Apulia, Southern Italy. *Palaeontographia Italica*, 88: 63-75.

Carus C.G. (1847). Resultate geologischer, anatomischer und zoologischer Untersuchungen über das unter dem Namen Hydrarchos von Dr. A. C. Koch, zuerst nach Europa gebrachte und in Dresden ausgestellte grofse fossile Skelett. 15 pp. Arnoldische Buchhandlung, Dresden.

Chesi F., Delfino M., Varola A. & Rook L. (2007). Fossil sea turtles (Chelonii, Dermochelyidae and Cheloniidae) from the Miocene of Pietra Leccese (late Burdigalian-early Messinian), Southern Italy. *Geodiversitas*, 29: 321-333.

Cipriano F. (2018). Atlantic White-Sided Dolphin. *In* Würsig B., Thewissen J.G.M. & Kovacs K.M. (eds), Encyclopedia of Marine Mammals, Third Edition, Academic Press: 42-44.

Collareta A., Fulgosi F.C. & Bianucci G. (2019a). A new kogiid sperm whale from northern Italy supports psychrospheric conditions in the early Pliocene Mediterranean Sea. *Acta Palaeontologica Polonica*, 64: 609-626.

Collareta A., Gemelli M., Varola A. & Bianucci G. (2019b). Trace fossils on a trace fossil: a vertebrate-bitten vertebrate coprolite from the Miocene of Italy. *Neues Jahrbuch für Geologie und Paläontologie, Abhandlungen*, 293: 117-126.

Collareta A., Lambert O., Muizon C. de, Benites-Palomino A., Urbina M. & Bianucci G. (2020). A new physeteroid from the late Miocene of Peru expands the diversity of extinct dwarf and pygmy sperm whales (Cetacea: Odontoceti: Kogiidae). *Comptes Rendus Palevol*, 19: 79-100.

Collareta A., Lambert O., Muizon C. de, Urbina M. & Bianucci G. (2017). *Koristocetus pescei* gen. et sp. nov., a diminutive sperm whale (Cetacea: Odontoceti: Kogiidae) from the late Miocene of Peru. *Fossil Record*, 20: 259-278.

Collareta A., Peri E., Carnevale G., Bosselaers M. & Bianucci G. (2021). On the presence of an ocean sunfish (Tetraodontiformes, Molidae) in the Miocene Pietra Leccese formation of Southern Italy. *Neues Jahrbuch für Geologie und Paläontologie, Abhandlungen*, 301: 147-155.

Collareta A., Peri E., Godfrey S.J. & Bianucci G. (in press). Just a different place to graze? An unusual occurrence of the echinoid feeding trace *Gnathichnus pentax* on a marine vertebrate coprolite (Miocene, Italy) and its palaeoethological implications. *Carnets Geol*, in press.

Cope E.D. (1867). An addition to the vertebrate fauna of the Miocene Period, with a synopsis of the extinct Cetacea of the United States. *Proceedings of the Academy of Natural Sciences of Philadelphia*, 19: 56-138.

Desmarest A.G. (1822). Mammalogie ou description des espèces de mammifères. Seconde partie. 555 pp. Mme veuve Agasse, Paris.

Du Bus B.A.L. (1867). Sur quelques mammifères du Crag d'Anvers. *Bulletins de l'Académie Royale des Sciences, des Lettres et des Beaux-Arts de Belgique*, 24: 562-577.

Du Bus B.A.L. (1872). Mammifères nouveaux du Crag d'Anvers. *Bulletin de l'Académie Royale des Sciences, des Lettres et des Beaux-Arts de Belgique*, 34: 491-509.

Evans K., Hindell M.A., Robertson K., Lockyer C. & Rice D. (2002). Factors affecting the precision of age determination of sperm whales (*Physeter macrocephalus*). *Journal of Cetacean Research and Management*, 4: 193-202.

Foresi L.M., Margiotta S. & Salvatorini G. (2002). Bio-cronostratigrafia a foraminiferi planctonici della Pietra leccese (Miocene) nell'area tipo di Cursi - Melpignano (Lecce, Puglia). *Bollettino della Società Paleontologica Italiana*, 41: 175-185.

Gervais P. (1861). Sur différentes espèces de vertébrés fossiles observées pour la plupart dans le midi de la France. *Mémoires de la Section des Sciences, Académie des Sciences et Lettres de Montpellier*, 8: 117-132.

Gill T. (1862). On the limits and arrangement of the family of scombroids. *Proceedings of the Academy of Natural Sciences of Philadelphia*, 14: 124-127.

Giménez J., Marçalo A., Ramírez F., Verborgh P., Gauffier P., Esteban R., Nicolau L., González-Ortegón E., Baldó F., Vilas C., Vingada J., Forero M.G. & de Stephanis R. (2017). Diet of bottlenose dolphins (*Tursiops truncatus*) from the Gulf of Cadiz: Insights from stomach content and stable isotope analyses. *PLOS ONE*, 12: e0184673.

Gondar D. (1975). La presencia de cetáceos Physeteridae en el Terciario Suprior ('Rionegrense') de la Provincia de Rio Negro. *Actas del Primer Congreso Argentino de Paleontología y Biostratigrafia Tucumán*, 2: 349-354.

Gray J.E. (1846). On the cetaceous animals. *In* Richardson J. & Gray J.E. (eds), The zoology of the voyage of the HMS. Erebus and Terror, under the command of Capt. Sir J. C. Ross, R. N., F. R. S., during the years 1839 to 1843. Vol. 1, part 3, Brown, Green and Longmans: 13-53.

Hampe O. (2006). Middle/late Miocene hoplocetine sperm whale remains (Odontoceti: Physeteridae) of North Germany with an emended classification of the Hoplocetinae. *Fossil Record*, 9: 61-86.

Hirota K. & Barnes L.G. (1994). A new species of Middle Miocene sperm whale of the genus *Scaldicetus* (Cetacea; Physeteridae) from Shiga-mura, Japan. *Island Arc*, 3: 453-472.

Huggenberger S., André M. & Oelschläger H.H.A. (2016). The nose of the sperm whale: overviews of functional design, structural homologies and evolution. *Journal of the Marine Biological Association of the United Kingdom*, 96: 783-806.

Kellogg R. (1925). On the occurrence of remains of fossil porpoises of the genus *Eurhinodelphis* in North America. *Proceedings of the United States National Museum*, 66: 1-40.

Kienle S.S., Law C.J., Costa D.P., Berta A. & Mehta R.S. (2017). Revisiting the behavioural framework of feeding in predatory aquatic mammals. *Proceedings of the Royal Society B: Biological Sciences*, 284 (1863): 20171035.

Kimura T. & Hasegawa Y. (2022). A New Physeteroid from the Lower Miocene of Japan. *Paleontological Research*, 26: 87-101.

Kimura T., Hasegawa Y. & Barnes L.G. (2006). Fossil sperm whales (Cetacea, Physeteridae) from Gunma and Ibaraki prefectures, Japan; with observations on the Miocene fossil sperm whale *Scaldicetus shigensis* Hirota and Barnes, 1995. *Bulletin of the Gunma Museum of Natural History*, 10: 1-23.

Kiszka J.J., Méndez-Fernandez P., Heithaus M.R. & Ridoux V. (2014). The foraging ecology of coastal bottlenose dolphins based on stable isotope mixing models and behavioural sampling. *Marine Biology*, 161: 953-961.

Kotsakis T., Delfino M. & Piras P. (2004). Italian Cenozoic crocodilians: taxa, timing and palaeobiogeographic implications. *Palaeogeography, Palaeoclimatology, Palaeoecology*, 210: 67-87.

Lacépède B.G.E. (1802). Histoire naturelle des poissons 4. 518 pp. Duménil, Paris.

Lambert O. (2004). Systematic revision of the Miocene long-snouted dolphin *Eurhinodelphis longirostris* du Bus, 1872 (Cetacea, Odontoceti, Eurhinodelphinidae). *Bulletin de l'Institut Royal des Sciences Naturelles de Belgique, Sciences de la Terre*, 74: 147-174.

Lambert O. (2008). Sperm whales from the Miocene of the North Sea: a re-appraisal. *Bulletin de l'Institut Royal Des Sciences Naturelles de Belgique, Sciences de La Terre*, 78: 277-316.

Lambert O. & Bianucci G. (2019). How to break a sperm whale's teeth: Dental damage in a large Miocene physeteroid from the North Sea Basin. *Journal of Vertebrate Paleontology*, 39: e1660987.

Lambert O., Bianucci G. & Beatty B.L. (2014). Bony outgrowths on the jaws of an extinct sperm whale support macroraptorial feeding in several stem physeteroids. *Naturwissenschaften*, 101: 517-521.

Lambert O., Bianucci G. & Muizon C. de (2008). A new stem-sperm whale (Cetacea, Odontoceti, Physeteroidea) from the Latest Miocene of Peru. *Comptes Rendus Palevol*, 7: 361-369.

Lambert O., Bianucci G. & Muizon C. de (2017). Macroraptorial sperm whales (cetacea, odontoceti, physeteroidea) from the Miocene of Peru. *Zoological Journal of the Linnean Society*, 179: 404-474.

Lambert O., Bianucci G., Post K., Muizon C. de, Salas-Gismondi R., Urbina M. & Reumer J. (2010). The giant bite of a new raptorial sperm whale from the Miocene epoch of Peru. *Nature*, 466: 105-108.

Lambert O., Muizon C. de, Urbina M. & Bianucci G. (2020). A new longirostrine sperm whale (Cetacea, Physeteroidea) from the lower Miocene of the Pisco Basin (southern coast of Peru). *Journal of Systematic Palaeontology*, 18: 1707-1742.

Lebeck H.J. (1801). *Delphinus delphis* beschrieben von Herrn Heinrich Julius Lebeck. *Der Gesellschaft Naturforschender Freunde zu Berlin, Neue Schriften*, 2: 280-282.

Leidy J. (1853). Observations on extinct Cetacea. *Proceedings of the Academy of Natural Sciences of Philadelphia*, 6: 377-378.

Linnaeus C. (1758). Systema Naturae sive Regna Tria Naturae, secundum Classes, Ordines, Genera, Species, cum characteribus, differentiis, synonymis, locis, Tomus I. Editio decima, reformata. 824 pp. Laurentius Salvius, Stockholm.

Lirer F., Foresi L.M., Iaccarino S.M., Salvatorini G., Turco E., Cosentino C., Sierro F.J. & Caruso A. (2019). Mediterranean Neogene planktonic foraminifer biozonation and biochronology. *Earth-Science Reviews*, 196: 102869.

Loch C., Grando L.J., Kieser J.A. & Simões-Lopes P.C. (2011). Dental pathology in dolphins (Cetacea: Delphinidae) from the southern coast of Brazil. *Diseases of Aquatic Organisms*, 94: 225-234.

Lydekker R. (1894). Cetacean skulls from Patagonia. *Anales del Museo de la Plata*, 2: 1-13.

Margiotta S. (2006). Bio-cronostratigrafia a foraminiferi planctonici dei sedimenti miocenici nell'area di Strudà (Lecce, Puglia). *Geologica Romana*, 39: 1-14.

Margiotta S. (2015). Inquadramento geologico e territoriale della pietra leccese. *Thalassia Salentina*, 37: 17-28.

Marra A.C., Carone G. & Bianucci G. (2016). Sperm whale teeth from the late Miocene of Cessaniti (Southern Italy). *Bollettino della Società Paleontologica Italiana*, 55: 223-225.

Martínez-Cáceres M. & Muizon C. de (2011). A new basilosaurid (Cetacea, Pelagiceti) from the late Eocene to early Oligocene Otuma Formation of Peru. *Comptes Rendus Palevol*, 10: 517-526.

Mazzei R., Margiotta S., Foresi L.M., Riforgiato F. & Salvatorini G. (2009). Biostratigraphy and chronostratigraphy of the Miocene Pietra Leccese in the type area of Lecce (Apulia, southern Italy). *Bollettino della Società Paleontologica Italiana*, 48: 129-145.

McAlpine D.F. (2018). Pygmy and Dwarf Sperm Whales. *In* Würsig B., Thewissen J.G.M. & Kovacs K.M. (eds), Encyclopedia of Marine Mammals, Third Edition, Academic Press: 786-788.

McCurry M.R. & Pyenson N.D. (2019). Hyper-longirostry and kinematic disparity in extinct toothed whales. *Paleobiology*, 45: 21-29.

Menesini E. (1969). Ittiodontoliti miocenici di Terra d'Otranto. *Palaeontographia Italica*, 65: 1-61.

Menesini E. & Tavani G. (1968). Resti di *Scaldicetus* (Cetacea) nel Miocene della Puglia. *Bollettino della Società Paleontologica Italiana*, 7: 87-93.

Møhl B., Madsen P.T., Wahlberg M., Au W.W.L., Nachtigall P.E. & Ridgway S.H. (2003). Sound transmission in the spermaceti complex of a recently expired sperm whale calf. *Acoustics Research Letters Online*, 4: 19-24.

Moncharmont Zei M. (1950). Sopra una nuova specie di *Eurhinodelphis* della Pietra leccese. *Rendiconti dell'Accademia di Scienze Fisiche e Matematiche della Società Nazionale di Scienze, Lettere ed Arti di Napoli*, 4: 1-11.

Moncharmont Zei M. (1956). *Hesperoina dalpiazi* n. gen. et n. sp., Platanistidae, Cetacea, della Pietra leccese. *Memorie Dell'Istituto di Geologia e Mineralogia dell'Università di Padova*, 19: 1-10.

Moreno F.P. (1892). Lijeros apuntes sobre dos géneros de cetáceos fósiles de la República Argentina. *Revista de la Museo La Plata*, 3: 393-400.

Muizon C. de (1988). Les vertébrés de la Formation Pisco (Pérou). Troisième partie: Les Odontocètes (Cetacea, Mammalia) du Miocène. *Travaux de l'Institut Français d'Etudes Andines*, 42: 1-244.

Müller J. (1849). Über die fossilen Reste der Zeuglodonten von Nordamerica. 38 pp. Verlag von G. Reimer, Berlin.

Owen R. (1866). On some Indian Cetacea collected by Walter Elliot, Esq. *Transactions of the Zoological Society of London*, 6: 17-47.

Paolucci F., Buono M.R., Fernández M.S., Marx F.G. & Cuitiño J.I. (2020). *Diaphorocetus poucheti* (Cetacea, Odontoceti, Physeteroidea) from Patagonia, Argentina: one of the earliest sperm whales. *Journal of Systematic Palaeontology*, 18: 335-355.

Paolucci F., Fernández M.S., Buono M.R. & Cuitiño J.I. (2021). '*Aulophyseter' rionegrensis* (Cetacea: Odontoceti: Physeteroidea) from the Miocene of Patagonia (Argentina): a reappraisal. *Zoological Journal of the Linnean Society*, 192: 1293-1322.

Peri E., Collareta A. & Bianucci G. (2020). A new record of physeteroidea from the upper Miocene of the Pietra leccese (southern Italy): systematics, paleoecology and taphonomy of a fossil macroraptorial sperm whale. *Rivista Italiana di Paleontologia e Stratigrafia*, 126: 751-769.

Peri E., Collareta A., Insacco G. & Bianucci G. (2019). An *Inticetus*-like (Cetacea: Odontoceti) postcanine tooth from the Pietra leccese (Miocene, southeastern Italy) and its palaeobiogeographical implications. *Neues Jahrbuch Fur Geologie Und Palaontologie - Abhandlungen*, 291: 221-228.

Peri E., Falkingham P.L., Collareta A. & Bianucci G. (2021). Biting in the Miocene seas: estimation of the bite force of the macroraptorial sperm whale *Zygophyseter varolai* using finite element analysis. *Historical Biology*: 1-12. doi: 10.1080/08912963.2021.1986814

Perrin W.F. (2018). Common Dolphin. *In* Würsig B., Thewissen J.G.M. & Kovacs K.M. (eds), Encyclopedia of Marine Mammals, Third Edition, Academic Press: 205-209.

Pilleri G. (1987). The Cetacea of the Italian Pliocene with a descriptive catalogue of the specimens in the Florence Museum of Paleontology. 160 pp. Brain Anatomy Institute, University of Berne, Berne.

Santos M., German I., Correia D., Read F., Martinez Cedeira J., Caldas M., López A., Velasco F. & Pierce G. (2013). Long-term variation in common dolphin diet in relation to prey abundance. *Marine Ecology Progress Series*, 481: 249-268.

Sorce B. (2009). Palaeontological study of the order Lamniformes in the Miocene Mediterranean Basin. 372 pp. PhD thesis, Università degli Studi di Pisa.

Staudinger M.D., McAlarney R.J., McLellan W.A. & Ann Pabst D. (2014). Foraging ecology and niche overlap in pygmy (*Kogia breviceps*) and dwarf (*Kogia sima*) sperm whales from waters of the U.S. mid-Atlantic coast. *Marine Mammal Science*, 30: 626-655.

Swofford D.L. (2002) PAUP* 4.0: Phylogenetic Analysis Using Parsimony (* and other methods). Sinauer Associates, Sunderland.

Tavani G. (1973). Ipotesi sulla presenza di grossi frammenti di gneiss e di calcare nella "pietra leccese" della Puglia. *Atti della Società Toscana di Scienze Naturali, Memorie Serie A*, 80: 121-125.

Van Beneden P.-J. (1869). Sur un nouveau genre de ziphioide fossile (*Placoziphius*), trouvé à Edeghem, près d'Anvers. *Mémoires de l'Académie Royale des Sciences, des Lettres et des Beaux-Arts de Belgique*, 37: 1-12.

Van Beneden P.-J. (1877). Note sur un Cachalot nain du crag d'Anvers (*Physeterula dubusii*). *Bulletin de l'Académie Royale des Sciences, des Lettres et des Beaux-Arts de Belgique*, 44: 851-856.

Vélez-Juarbe J., Wood A.R., De Gracia C. & Hendy A.J. (2015). Evolutionary patterns among living and fossil kogiid sperm whales: evidence from the Neogene of Central America. *PLOS ONE*, 10: e0123909.

Vigliarolo G. (1890). Monografia dei *Pristis* fossili con la descrizione di una nuova specie del calcare miocenico di Lecce. *Atti della Reale Accademia delle Scienze Fisiche e Matematiche di Napoli*, 4: 1-28.

von Meyer H. (1843). Mittheilungen an Professor Bronn gerichtet. *Neues Jahrbuch für Mineralogie, Geognosie, Geologie und Petrefaktenkunden*, 1843: 698-704.

von Meyer H. (1847). Mittheilungen an Professor Bronn gerichtet. *Neues Jahrbuch für Mineralogie, Geognosie, Geologie und Petrefaktenkunde*, 1847: 572-81.

Wang J.Y. (2018). Bottlenose Dolphin, *Tursiops aduncus*, Indo-Pacific Bottlenose Dolphin. *In* Würsig B., Thewissen J.G.M. & Kovacs K.M. (eds), Encyclopedia of Marine Mammals, Third Edition, Academic Press: 125-130.

Wells R.S. & Scott M.D. (2018). Bottlenose Dolphin, *Tursiops truncatus*, Common Bottlenose Dolphin. *In* Würsig B., Thewissen J.G.M. & Kovacs K.M. (eds), Encyclopedia of Marine Mammals, Third Edition, Academic Press: 118-125.

Werth A.J. (2004). Functional morphology of the sperm whale (*Physeter macrocephalus*) tongue, with reference to suction feeding. *Aquatic Mammals*, 30: 405-418.

Werth A.J. (2006a). Odontocete suction feeding: Experimental analysis of water flow and head shape. *Journal of Morphology*, 267: 1415-1428.

Werth A.J. (2006b). Mandibular and Dental Variation and the Evolution of Suction Feeding in Odontoceti. *Journal of Mammalogy*, 87: 579-588.

Wezel F.C. (1966). "*Globorotalia*" *acrostoma* nuova specie dell'Oligo-Miocene italiano. *Rivista Italiana di Paleontologia e Stratigrafia*, 72: 1297-1312.

Whitehead H. (2018). Sperm Whale. *In* Würsig B., Thewissen J.G.M. & Kovacs K.M. (eds), Encyclopedia of Marine Mammals, Third Edition, Academic Press: 919-925.

Whitmore F.C. Jr. & Kaltenbach J.A. (2008). Neogene Cetacea of the Lee Creek Phosphate Mine, North Carolina. *In* Ray C.E., Bohaska D.J., Koretsky I.A., Ward L.W. & Barnes L.G. (eds), Geology and Paleontology of the Lee Creek Mine, North Carolina, IV, *Virginia Museum of Natural History Special Publication*, 14: 181-269.

Manuscript received 30 June 2022
Revised manuscript accepted 6 August 2022
Zoobank registration date 17 August 2022
Zoobank registration number: *urn:lsid:zoobank.org:pub:641FDCA7-111E-45AE-9BAE-E92C4AD89178*
Published online 13 September 2022
Guest Editor Giorgio Carnevale